Z. Phys. C 71, 11–30 (1996)

ZEITSCHRIFT
FÜR PHYSIK C

Mean lifetime of the B_s^0 meson

DELPHI Collaboration

P.Abreu[21], W.Adam[50], T.Adye[37], E.Agasi[31], I.Ajinenko[42], R.Aleksan[39], G.D.Alekseev[16], R.Alemany[49], P.P.Allport[22], S.Almehed[24], U.Amaldi[9], S.Amato[47], A.Andreazza[28], M.L.Andrieux[14], P.Antilogus[9], W-D.Apel[17], Y.Arnoud[39], B.Åsman,[44], J-E.Augustin[25], A.Augustinus[9], P.Baillon[9], P.Bambade[19], F.Barao[21], R.Barate[14], M.Barbi[47], G.Barbiellini[46], D.Y.Bardin[16], A.Baroncelli[40], O.Barring[24], J.A.Barrio[26], W.Bartl[50], M.J.Bates[37], M.Battaglia[15], M.Baubillier[23], J.Baudot[39], K-H.Becks[52], M.Begalli[6], P.Beilliere[8], Yu.Belokopytov[9,⋆], A.C.Benvenuti[5], M.Berggren[47], D.Bertrand[2], F.Bianchi[45], M.Bigi[45], M.S.Bilenky[16], P.Billoir[23], D.Bloch[10], M.Blume[52], S.Blyth[35], T.Bolognese[39], M.Bonesini[28], W.Bonivento[28], P.S.L.Booth[22], G.Borisov[42], C.Bosio[40], S.Bosworth[35], O.Botner[48], E.Boudinov[31], B.Bouquet[19], C.Bourdarios[9], T.J.V.Bowcock[22], M.Bozzo[13], P.Branchini[40], K.D.Brand[36], T.Brenke[52], R.A.Brenner[15], C.Bricman[2], L.Brillault[23], R.C.A.Brown[9], P.Bruckman[18], J-M.Brunet[8], L.Bugge[33], T.Buran[33], T.Burgsmueller[52], P.Buschmann[52], A.Buys[9], S.Cabrera[49], M.Caccia[28], M.Calvi[28], A.J.Camacho Rozas[41], T.Camporesi[9], V.Canale[38], M.Canepa[13], K.Cankocak[44], F.Cao[2], F.Carena[9], L.Carroll[22], C.Caso[13], M.V.Castillo Gimenez[49], A.Cattai[9], F.R.Cavallo[5], L.Cerrito[38], V.Chabaud[9], M.Chapkin[42], Ph.Charpentier[9], L.Chaussard[25], J.Chauveau[23], P.Checchia[36], G.A.Chelkov[16], M.Chen[2], R.Chierici[45], P.Chliapnikov[42], P.Chochula[7], V.Chorowicz[9], J.Chudova[30], V.Cindro[43], P.Collins[9], J.L.Contreras[19], R.Contri[13], E.Cortina[49], G.Cosme[19], F.Cossutti[46], H.B.Crawley[1], D.Crennell[37], G.Crosetti[13], J.Cuevas Maestro[34], S.Czellar[15], E.Dahl-Jensen[29], J.Dahm[52], B.Dalmagne[19], M.Dam[29], G.Damgaard[29], P.D.Dauncey[37], M.Davenport[9], W.Da Silva[23], C.Defoix[8], A.Deghorain[2], G.Della Ricca[46], P.Delpierre[27], N.Demaria[35], A.De Angelis[9], W.De Boer[17], S.De Brabandere[2], C.De Clercq[2], C.De La Vaissiere[23], B.De Lotto[46], A.De Min[36], L.De Paula[47], C.De Saint-Jean[39], H.Dijkstra[9], L.Di Ciaccio[38], F.Djama[10], J.Dolbeau[8], M.Donszelmann[9], K.Doroba[51], M.Dracos[10], J.Drees[52], K.-A.Drees[52], M.Dris[32], D.Edsall[1], R.Ehret[17], G.Eigen[4], T.Ekelof[48], G.Ekspong[44], M.Elsing[52], J-P.Engel[10], N.Ershaidat[23], B.Erzen[43], M.Espirito Santo[21], E.Falk[24], D.Fassouliotis[32], M.Feindt[9], A.Fenyuk[42], A.Ferrer[49], T.A.Filippas[32], A.Firestone[1], P.-A.Fischer[10], H.Foeth[9], E.Fokitis[32], F.Fontanelli[13], F.Formenti[9], B.Franek[37], P.Frenkiel[8], D.C.Fries[17], A.G.Frodesen[4], R.Fruhwirth[50], F.Fulda-Quenzer[19], J.Fuster[49], A.Galloni[22], D.Gamba[45], M.Gandelman[6], C.Garcia[49], J.Garcia[41], C.Gaspar[9], U.Gasparini[36], Ph.Gavillet[9], E.N.Gazis[32], D.Gele[10], J-P.Gerber[10], M.Gibbs[22], R.Gokieli[51], B.Golob[43], G.Gopal[37], L.Gorn[1], M.Gorski[51], Yu.Gouz[45,⋆], V.Gracco[13], E.Graziani[40], G.Grosdidier[19], K.Grzelak[51], S.Gumenyuk[28,⋆], P.Gunnarsson[44], M.Gunther[48], J.Guy[37], F.Hahn[9], S.Hahn[52], Z.Hajduk[18], A.Hallgren[48], K.Hamacher[52], W.Hao[31], F.J.Harris[35], V.Hedberg[24], R.Henriques[21], J.J.Hernandez[49], P.Herquet[2], H.Herr[9], T.L.Hessing[35], E.Higon[49], H.J.Hilke[9], T.S.Hill[1], S-O.Holmgren[44], P.J.Holt[35], D.Holthuizen[31], S.Hoorelbeke[2], M.Houlden[22], K.Huet[2], K.Hultqvist[44], J.N.Jackson[22], R.Jacobsson[44], P.Jalocha[18], R.Janik[7], Ch.Jarlskog[24], G.Jarlskog[24], P.Jarry[39], B.Jean-Marie[19], E.K.Johansson[44], L.Jonsson[24], P.Jonsson[24], C.Joram[9], P.Juillot[10], M.Kaiser[17], F.Kapusta[23], K.Karafasoulis[11], M.Karlsson[44], E.Karvelas[11], S.Katsanevas[3], E.C.Katsoufis[32], R.Keranen[4], B.A.Khomenko[16], N.N.Khovanski[16], B.King[22], N.J.Kjaer[29], H.Klein[9], A.Klovning[4], P.Kluit[31], B.Koene[31], P.Kokkinias[11], M.Koratzinos[9], K.Korcyl[18], V.Kostioukhine[42], C.Kourkoumelis[3], O.Kouznetsov[13,16], P.-H.Kramer[52], M.Krammer[50], C.Kreuter[17], I.Kronkvist[24], Z.Krumstein[16], W.Krupinski[18], P.Kubinec[7], W.Kucewicz[18], K.Kurvinen[15], C.Lacasta[49], I.Laktineh[25], S.Lamblot[23], J.W.Lamsa[1], L.Lanceri[46], D.W.Lane[1], P.Langefeld[52], V.Lapin[42], I.Last[22], J-P.Laugier[39], R.Lauhakangas[15], G.Leder[50], F.Ledroit[14], V.Lefebure[2], C.K.Legan[1], R.Leitner[30], Y.Lemoigne[39], J.Lemonne[2], G.Lenzen[52], V.Lepeltier[19], T.Lesiak[36], D.Liko[50], R.Lindner[52], A.Lipniacka[36], I.Lippi[36], B.Loerstad[24], J.G.Loken[35], J.M.Lopez[41], D.Loukas[11], P.Lutz[39], L.Lyons[35], J.MacNaughton[50], G.Maehlum[17], A.Maio[21], V.Malychev[16], F.Mandl[50], J.Marco[41], R.Marco[41], B.Marechal[47], M.Margoni[36], J-C.Marin[9], C.Mariotti[40], A.Markou[11], T.Maron[52], C.Martinez-Rivero[41], F.Martinez-Vidal[49], S.Marti i Garcia[49], J.Masik[30], F.Matorras[41], C.Matteuzzi[9], G.Matthiae[38], M.Mazzucato[36], M.Mc Cubbin[9], R.Mc Kay[1], R.Mc Nulty[22], J.Medbo[48], M.Merk[31], C.Meroni[28], S.Meyer[17], W.T.Meyer[1], M.Michelotto[36], E.Migliore[45], L.Mirabito[25], W.A.Mitaroff[50], U.Mjoernmark[24], T.Moa[44], R.Moeller[29], K.Moenig[9], M.R.Monge[13], P.Morettini[13], H.Mueller[17], L.M.Mundim[6], W.J.Murray[37], B.Muryn[18], G.Myatt[35], F.Naraghi[14], F.L.Navarria[5], S.Navas[49], K.Nawrocki[51], P.Negri[28], W.Neumann[52], N.Neumeister[50], R.Nicolaidou[3], B.S.Nielsen[29], M.Nieuwenhuizen[31], V.Nikolaenko[10], P.Niss[44], A.Nomerotski[36], A.Normand[35], M.Novak[12], W.Oberschulte-Beckmann[17], V.Obraztsov[42], A.G.Olshevski[16], A.Onofre[21], R.Orava[15], A.Ostankov[42], K.Osterberg[15], A.Ouraou[39], P.Paganini[19], M.Paganoni[9], P.Pages[10], H.Palka[18], Th.D.Papadopoulou[32], K.Papageorgiou[11], L.Pape[9], C.Parkes[35], F.Parodi[13], A.Passeri[40], M.Pegoraro[36], H.Pernegger[50], M.Pernicka[50], A.Perrotta[5], C.Petridou[46], A.Petrolini[13], M.Petrovyck[28,⋆], H.T.Phillips[37], G.Piana[13], F.Pierre[39], M.Pimenta[21], M.Pindo[28], S.Plaszczynski[19], O.Podobrin[17], M.E.Pol[6], G.Polok[18], P.Poropat[46], V.Pozdniakov[16], M.Prest[46], P.Privitera[38], N.Pukhaeva[16], A.Pullia[28], D.Radojicic[35], S.Ragazzi[28], H.Rahmani[32], P.N.Ratoff[20], A.L.Read[33], M.Reale[52], P.Rebecchi[19], N.G.Redaelli[28], M.Regler[50], D.Reid[9], P.B.Renton[35], L.K.Resvanis[3], F.Richard[19], J.Richardson[22], J.Ridky[12], G.Rinaudo[45], I.Ripp[39], A.Romero[45], I.Roncagliolo[13], P.Ronchese[36], L.Roos[14], E.I.Rosenberg[1], E.Rosso[9], P.Roudeau[19], T.Rovelli[5], W.Ruckstuhl[31], V.Ruhlmann-Kleider[39], A.Ruiz[41], K.Rybicki[18],

H.Saarikko[15], Y.Sacquin[39], A.Sadovsky[16], G.Sajot[14], J.Salt[49], J.Sanchez[26], M.Sannino[13], M.Schimmelpfennig[17], H.Schneider[17], U.Schwickerath[17], M.A.E.Schyns[52], G.Sciolla[45], F.Scuri[46], P.Seager[20], Y.Sedykh[16], A.M.Segar[35], A.Seitz[17], R.Sekulin[37], R.C.Shellard[6], I.Siccama[31], P.Siegrist[39], S.Simonetti[39], F.Simonetto[36], A.N.Sisakian[16], B.Sitar[7], T.B.Skaali[33], G.Smadja[25], N.Smirnov[42], O.Smirnova[24], G.R.Smith[37], R.Sosnowski[51], D.Souza-Santos[6], T.Spassov[21], E.Spiriti[40], P.Sponholz[52], S.Squarcia[13], C.Stanescu[40], S.Stapnes[33], I.Stavitski[36], F.Stichelbaut[9], A.Stocchi[19], J.Strauss[50], R.Strub[10], B.Stugu[4], M.Szczekowski[51], M.Szeptycka[51], T.Tabarelli[28], J.P.Tavernet[23], O.Tchikilev[42], A.Tilquin[27], J.Timmermans[31], L.G.Tkatchev[16], T.Todorov[10], S.Todorova[10], D.Z.Toet[31], A.Tomaradze[2], B.Tome[21], A.Tonazzo[28], L.Tortora[40], G.Transtromer[24], D.Treille[9], W.Trischuk[9], G.Tristram[8], A.Trombini[19], C.Troncon[28], A.Tsirou[9], M-L.Turluer[39], I.A.Tyapkin[16], M.Tyndel[37], S.Tzamarias[22], B.Ueberschaer[52], O.Ullaland[9], V.Uvarov[42], G.Valenti[5], E.Vallazza[9], C.Vander Velde[2], G.W.Van Apeldoorn[31], P.Van Dam[31], W.K.Van Doninck[2], J.Van Eldik[31], N.Vassilopoulos[35], G.Vegni[28], L.Ventura[36], W.Venus[37], F.Verbeure[2], M.Verlato[36], L.S.Vertogradov[16], D.Vilanova[39], P.Vincent[25], L.Vitale[46], E.Vlasov[42], A.S.Vodopyanov[16], V.Vrba[12], H.Wahlen[52], C.Walck[44], M.Weierstall[52], P.Weilhammer[9], C.Weiser[17], A.M.Wetherell[9], D.Wicke[52], J.H.Wickens[2], M.Wielers[17], G.R.Wilkinson[35], W.S.C.Williams[35], M.Winter[10], M.Witek[18], K.Woschnagg[48], K.Yip[35], F.Zach[25], A.Zaitsev[42], A.Zalewska[18], P.Zalewski[51], D.Zavrtanik[43], E.Zevgolatakos[11], N.I.Zimin[16], M.Zito[39], D.Zontar[43], R.Zuberi[35], G.C.Zucchelli[44], G.Zumerle[36]

[1] Ames Laboratory and Department of Physics, Iowa State University, Ames IA 50011, USA
[2] Physics Department, Univ. Instelling Antwerpen, Universiteitsplein 1, B-2610 Wilrijk, Belgium
and IIHE, ULB-VUB, Pleinlaan 2, B-1050 Brussels, Belgium
and Faculté des Sciences, Univ. de l'Etat Mons, Av. Maistriau 19, B-7000 Mons, Belgium
[3] Physics Laboratory, University of Athens, Solonos Str. 104, GR-10680 Athens, Greece
[4] Department of Physics, University of Bergen, Allégaten 55, N-5007 Bergen, Norway
[5] Dipartimento di Fisica, Università di Bologna and INFN, Via Irnerio 46, I-40126 Bologna, Italy
[6] Centro Brasileiro de Pesquisas Físicas, rua Xavier Sigaud 150, RJ-22290 Rio de Janeiro, Brazil
and Depto. de Física, Pont. Univ. Católica, C.P. 38071 RJ-22453 Rio de Janeiro, Brazil
and Inst. de Física, Univ. Estadual do Rio de Janeiro, rua São Francisco Xavier 524, Rio de Janeiro, Brazil
[7] Comenius University, Faculty of Mathematics and Physics, Mlynska Dolina, SK-84215 Bratislava, Slovakia
[8] Collège de France, Lab. de Physique Corpusculaire, IN2P3-CNRS, F-75231 Paris Cedex 05, France
[9] CERN, CH-1211 Geneva 23, Switzerland
[10] Centre de Recherche Nucléaire, IN2P3 - CNRS/ULP - BP20, F-67037 Strasbourg Cedex, France
[11] Institute of Nuclear Physics, N.C.S.R. Demokritos, P.O. Box 60228, GR-15310 Athens, Greece
[12] FZU, Inst. of Physics of the C.A.S. High Energy Physics Division, Na Slovance 2, 180 40, Praha 8, Czech Republic
[13] Dipartimento di Fisica, Università di Genova and INFN, Via Dodecaneso 33, I-16146 Genova, Italy
[14] Institut des Sciences Nucléaires, IN2P3-CNRS, Université de Grenoble 1, F-38026 Grenoble Cedex, France
[15] Research Institute for High Energy Physics, SEFT, P.O. Box 9, FIN-00014 Helsinki, Finland
[16] Joint Institute for Nuclear Research, Dubna, Head Post Office, P.O. Box 79, 101 000 Moscow, Russian Federation
[17] Institut für Experimentelle Kernphysik, Universität Karlsruhe, Postfach 6980, D-76128 Karlsruhe, Germany
[18] Institute of Nuclear Physics and University of Mining and Metalurgy, Ul. Kawiory 26a, PL-30055 Krakow, Poland
[19] Université de Paris-Sud, Lab. de l'Accélérateur Linéaire, IN2P3-CNRS, Bât. 200, F-91405 Orsay Cedex, France
[20] School of Physics and Materials, University of Lancaster, Lancaster LA1 4YB, UK
[21] LIP, IST, FCUL - Av. Elias Garcia, 14-1^{o}, P-1000 Lisboa Codex, Portugal
[22] Department of Physics, University of Liverpool, P.O. Box 147, Liverpool L69 3BX, UK
[23] LPNHE, IN2P3-CNRS, Universités Paris VI et VII, Tour 33 (RdC), 4 place Jussieu, F-75252 Paris Cedex 05, France
[24] Department of Physics, University of Lund, Sölvegatan 14, S-22363 Lund, Sweden
[25] Université Claude Bernard de Lyon, IPNL, IN2P3-CNRS, F-69622 Villeurbanne Cedex, France
[26] Universidad Complutense, Avda. Complutense s/n, E-28040 Madrid, Spain
[27] Univ. d'Aix - Marseille II - CPP, IN2P3-CNRS, F-13288 Marseille Cedex 09, France
[28] Dipartimento di Fisica, Università di Milano and INFN, Via Celoria 16, I-20133 Milan, Italy
[29] Niels Bohr Institute, Blegdamsvej 17, DK-2100 Copenhagen 0, Denmark
[30] NC, Nuclear Centre of MFF, Charles University, Areal MFF, V Holesovickach 2, 180 00, Praha 8, Czech Republic
[31] NIKHEF-H, Postbus 41882, NL-1009 DB Amsterdam, The Netherlands
[32] National Technical University, Physics Department, Zografou Campus, GR-15773 Athens, Greece
[33] Physics Department, University of Oslo, Blindern, N-1000 Oslo 3, Norway
[34] Dpto. Fisica, Univ. Oviedo, C/P. Pérez Casas, S/N-33006 Oviedo, Spain
[35] Department of Physics, University of Oxford, Keble Road, Oxford OX1 3RH, UK
[36] Dipartimento di Fisica, Università di Padova and INFN, Via Marzolo 8, I-35131 Padua, Italy
[37] Rutherford Appleton Laboratory, Chilton, Didcot OX11 OQX, UK
[38] Dipartimento di Fisica, Università di Roma II and INFN, Tor Vergata, I-00173 Rome, Italy
[39] Centre d'Etudes de Saclay, DSM/DAPNIA, F-91191 Gif-sur-Yvette Cedex, France
[40] Istituto Superiore di Sanità, Ist. Naz. di Fisica Nucl. (INFN), Viale Regina Elena 299, I-00161 Rome, Italy
[41] Instituto de Fisica de Cantabria (CSIC-UC), Avda. los Castros, S/N-39006 Santander, Spain, (CICYT-AEN93-0832)
[42] Inst. for High Energy Physics, Serpukov P.O. Box 35, Protvino, (Moscow Region), Russian Federation
[43] J. Stefan Institute and Department of Physics, University of Ljubljana, Jamova 39, SI-61000 Ljubljana, Slovenia
[44] Fysikum, Stockholm University, Box 6730, S-113 85 Stockholm, Sweden
[45] Dipartimento di Fisica Sperimentale, Università di Torino and INFN, Via P. Giuria 1, I-10125 Turin, Italy
[46] Dipartimento di Fisica, Università di Trieste and INFN, Via A. Valerio 2, I-34127 Trieste, Italy
and Istituto di Fisica, Università di Udine, I-33100 Udine, Italy
[47] Univ. Federal do Rio de Janeiro, C.P. 68528 Cidade Univ., Ilha do Fundão BR-21945-970 Rio de Janeiro, Brazil

[48] Department of Radiation Sciences, University of Uppsala, P.O. Box 535, S-751 21 Uppsala, Sweden
[49] IFIC, Valencia-CSIC, and D.F.A.M.N., U. de Valencia, Avda. Dr. Moliner 50, E-46100 Burjassot (Valencia), Spain
[50] Institut für Hochenergiephysik, Österr. Akad. d. Wissensch., Nikolsdorfergasse 18, A-1050 Vienna, Austria
[51] Inst. Nuclear Studies and University of Warsaw, Ul. Hoza 69, PL-00681 Warsaw, Poland
[52] Fachbereich Physik, University of Wuppertal, Postfach 100 127, D-42097 Wuppertal, Germany

⋆ On leave of absence from IHEP Serpukhov

Received: 11 March 1996

Abstract. This paper presents an update of the measurement of the mean lifetime of the B_s^0 meson. Combining $D_s - \ell$, $D_s - h$, $\phi - \ell$ and inclusive D_s final states from the 3.2 million hadronic Z decays collected by DELPHI between 1991 and 1994, the B_s^0 mean lifetime was measured to be: $\tau(B_s^0)$ = 1.67 $\pm$ 0.14 ps.

1 Introduction

During the hadronisation of b quark jets emitted from a Z boson decay $\overline{\mathrm{B}}_\mathrm{s}^0$ mesons, composed of a b and an $\overline{s}$ quark, are produced when the b quark combines with a strange antiquark from an $s\overline{s}$ pair. [1] Since the probability of this occurring in a b quark jet is only about 10%, fewer $\overline{\mathrm{B}}_\mathrm{s}^0$ mesons are produced than non-strange $\overline{\mathrm{B}}$ mesons. To measure the mean $\overline{\mathrm{B}}_\mathrm{s}^0$ lifetime, decay channels which allow good rejection of non-strange $\overline{\mathrm{B}}$ hadrons must therefore be used. In this paper, four different selections have been used to obtain enriched samples in which the $\overline{\mathrm{B}}_\mathrm{s}^0$ purity (*i.e.* the fraction of $\overline{\mathrm{B}}_\mathrm{s}^0$ decays in the selected $\overline{\mathrm{B}}$ hadron decays) lies between 50% and 90%.

The first method (Sect. 3) uses D_s^+ mesons correlated with a lepton (ℓ, here meaning a muon or electron) of opposite charge (*i.e.* ℓ^-) produced in the same hemisphere. Requiring a lepton with large momentum transverse to the jet axis suppresses both indirect semileptonic $\overline{\mathrm{B}}$ meson decays ($b \to c \to \ell^+$) and fake leptons (due to light hadrons decaying to a lepton or being misidentified as a lepton). A high $\overline{\mathrm{B}}_\mathrm{s}^0$ purity is obtained by requiring the presence of a D_s^+ meson, which are produced more frequently in $\overline{\mathrm{B}}_\mathrm{s}^0$ than in $\overline{\mathrm{B}}_d^0$ or B^- semileptonic decays because the spectator $\overline{s}$ quark needed is already present in the $\overline{\mathrm{B}}_\mathrm{s}^0$ meson. Requiring both a high transverse momentum ℓ^- and a D_s^+ with the correct charge correlation ("right-sign"[2]) provides a sample in which about 90 % originate from $\overline{\mathrm{B}}_\mathrm{s}^0$ semileptonic decays.

The second method (Sect. 4) uses events containing a D_s^+ meson and a hadron of high momentum and opposite charge (h^-). D_s^+ mesons can originate from the hadronization of charm quarks in $\mathrm{Z} \to c\overline{c}$ decays, from decays of non-strange $\overline{\mathrm{B}}$ hadrons which produce D_s^+ mainly in processes with two charmed hadrons in the final state, like $\mathrm{B_{d,u}} \to \mathrm{D_s}^{(\star)}\overline{\mathrm{D}}^{(\star)}\mathrm{X}$, and from $\overline{\mathrm{B}}_\mathrm{s}^0$ decays. Selecting events with certain kinematic cuts gives a sample of events with a $\overline{\mathrm{B}}_\mathrm{s}^0$ purity of about 60%.

The third analysis (Sect. 5) is more inclusive and concerns events in which a high transverse momentum lepton is accompanied by a ϕ meson in the same jet. Inclusive production rates of ϕ mesons in D^0, D^+ and D_s^+ decays have not been yet measured. Nevertheless it has been shown [1] that the inclusive rates can be inferred with reasonable accuracy from the measured exclusive decays. The high transverse momentum lepton enriches the sample in direct semileptonic decays and the presence of the ϕ enriches its $\overline{\mathrm{B}}_\mathrm{s}^0$ purity to around 50%.

The fourth analysis (Sect. 6) uses events containing simply a D_s^+ meson. This approach provides high statistics of D_s^+, but the estimates of the energy and of the flight distance of the $\overline{\mathrm{B}}_\mathrm{s}^0$ are less accurate than in the other analyses and some 30% of the selected D_s^+ are from $\mathrm{Z} \to c\overline{c}$ decays. The $\overline{\mathrm{B}}_\mathrm{s}^0$ purity of the rest of the sample is around 55%.

The events used in these analyses correspond to about 3.2 million hadronic Z decays recorded by DELPHI in 1991-1994. The rates and other quantities used in the calculation of the different processes are given in Table 2. Additional details are given in the text.

2 Event selection and particle identification

The events used in this analysis were collected at LEP running at the Z resonance with the DELPHI detector [11], whose performance is detailed in [12]. Hadronic decays of the Z were selected with standard cuts on multiplicity and energy with an efficiency close to 95 % [12]. Each selected event was divided into two hemispheres separated by the plane transverse to the sphericity axis. A clustering analysis based on the JETSET algorithm LUCLUS with default parameters was used to define jets using both charged and neutral particles [13]. These jets were used to compute the p_t^{out} of each particle of the event as its momentum transverse to the axis of the rest of the jet it belonged to, *i.e.* to the jet axis recomputed after removing the particle from the jet.

Simulated events were generated using the JETSET parton shower model [13] and analysed in the same way as the real data events. The JETSET parameters were adjusted from previous studies [14]. Semileptonic B hadron decays were simulated using the ISGW [15] model with a fraction of 30% for D^{**} production. Full simulation of the detector response was included [16].

In DELPHI, lepton identification is based on the muon chambers and the electromagnetic calorimeters, charged

[1] In this paper, unless explicitly stated otherwise, corresponding statements for charge conjugate states are always implied

[2] Pairs satisfying this opposite-charge correlation will often be called "right-sign", while the expression "wrong-sign" will be used for D_s^+ mesons with leptons of the same charge; the same terminology is used in the second analysis (D_s^+-h^-)

Table 1. Production rates and other measured quantities used in the various analyses. Both P_s and $P_{u,d}$ were deduced from the measurements [7] of the average mixing probability $\bar{\chi}$ at LEP and of the B_d mixing probability χ_d obtained at LEP and at the $\Upsilon(4S)$, taken together with the limit on the B_s mixing probability χ_s and the value of P_{baryon}. The latter was taken from measurements of Λ_c production in c jets [8], assuming that it is similar for Λ_b in b jets and using a production rate of $(2 \pm 2)\%$ for strange B baryon states

Measured quantities	Value	Reference
B_1 = Br($b \to \overline{B}^0_s \to D^+_s \ell^- \overline{\nu}$) $\times$ Br($D^+_s \to \phi\pi^+$)	$(3.1 \pm 0.5) \times 10^{-4}$	[2]
B_2 = Br($B_{u,d} \to D^\pm_s X$) $\times$ Br($D^\pm_s \to \phi\pi^\pm$)	$(3.66 \pm 0.22) \times 10^{-3}$	[3]
B_L = Br($b \to D^\pm_s X$) $\times$ Br($D^\pm_s \to \phi\pi^\pm$)	$(0.72 \pm 0.09) \times 10^{-2}$	[4]
B_3 = Br($b \to \overline{B}^0_s \to D^\pm_s X$) $\times$ Br($D^\pm_s \to \phi\pi^\pm$)	$(0.39 \pm 0.09) \times 10^{-2}$	[4]
B_4 = $P(c \to D^+_s)$ $\times$ Br($D^+_s \to \phi\pi^+$)	$(0.32 \pm 0.04) \times 10^{-2}$	[5]
B_{bcl} = Br($b \to c \to \bar{\ell}$)	$(8.22 \pm 0.42) \times 10^{-2}$	[6]
Br($b \to \ell$)	$(10.43 \pm 0.24) \times 10^{-2}$	[6]
$P_{u,d}$ = Br($b \to B^-_u$) = Br($b \to \overline{B}^0_d$)	0.392 ± 0.022	[7]
P_s = Br($b \to \overline{B}^0_s$)	0.100 ± 0.022	[7]
P_{baryon} = Br($b \to B_{baryon}$)	0.116 ± 0.032	[8]
$R_{b\bar{b}} = \Gamma_{Z\to b\bar{b}} \,/\, \Gamma_{Z\to Hadrons}$	0.2202 ± 0.0020	[6]
$R_{c\bar{c}} = \Gamma_{Z\to c\bar{c}} \,/\, \Gamma_{Z\to Hadrons}$	0.1583 ± 0.0098	[6]
$P(c \to D^+)$	0.248 ± 0.037	[9]
$P(b \to D^+)$	$0.246 \pm 0.031 \pm 0.025$	[10]
Br($D^+_s \to \phi X$)	$(4.8 \pm 0.5) \times$ Br($D^+_s \to \phi\pi^+$)	[1]
Br($D^0 \to \phi X$)	$(1.8 \pm 0.3) \times 10^{-2}$	[1]
Br($D^+ \to \phi X$)	$(1.7 \pm 0.3) \times 10^{-2}$	[1]

hadron identification is performed using the Ring Image CHerenkov (RICH) detectors and the Time Projection Chamber (TPC), and the Vertex Detector (VD) is used in combination with the central tracking devices to measure the charged particle trajectories close to the beam interaction point very precisely and thus to identify the charged particles coming from B or D meson decays.

The DELPHI reference frame is defined with z along the e^- beam, x towards the centre of LEP and y upwards. The angular coordinates are the polar angle θ, measured from the z-axis, and the azimuth, ϕ, measured from the x-axis, while R is the distance from the z-axis.

The muon chambers are drift chambers located at the periphery of DELPHI. The barrel part ($-0.63 < \cos(\theta) < 0.63$) is composed of three sets of modules, each with two active layers, and gives z and $R\phi$ coordinates. In the forward part, two layers of two planes give the x and y coordinates in the transverse plane. The precision of these detectors has to be taken into account for muon identification: it has been measured to be ± 1 cm in z and ± 0.2 cm in $R\phi$ for the barrel part, and ± 0.4 cm for each of the two coordinates given by the forward part. The number of absorption lengths determines the hadron contamination and has a minimum of approximately 8 absorption lengths at 90°. The muon identification algorithm is described in [12]. Loose selection criteria provided an identification efficiency within the acceptance of the muon chambers of 95 % for a probability of misidentifying a pion as a muon of about 1.5%. Tighter cuts gave 76 % efficiency for a misidentification probability of 0.44 %.

Electrons are absorbed in the electromagnetic calorimeters. The High density Projection Chamber (HPC) covers the barrel part and provides three-dimensional information on electromagnetic showers with a thickness of 18 radiation lengths. Calorimeters in the endcap regions are not used in this analysis because their angular acceptance lies outside the solid angle covered by the VD. The electron identification algorithm is described in [12]. Inside the angular acceptance of the HPC, electrons of momentum above 3 GeV/c were identified with an efficiency of 77 ± 2 %. The probability of a pion being misidentified as an electron was below 1 %.

Charged hadron identification relies on the RICH detector and on the energy loss, dE/dx, measured in the TPC. The 192 sense wires of the TPC measure the specific energy loss of charged particles as the 80% truncated mean of the amplitudes of the wire signals, with a minimum requirement of 30 wires. This dE/dx measurement is available for 75% of charged particles in hadronic jets, with a precision which has been measured to be $\pm$6.7% in the momentum range $4 < p < 25$ GeV/c . The RICH detector consists of two parts: a liquid radiator and a gas radiator. The liquid radiator provides complete $p/\mathrm{K}/\pi$ separation in the momentum range 2.5 – 8 GeV/c by measuring the Cherenkov angle with an average precision of 13 mrad. In this momentum range the gas radiator operates in the "veto" mode (kaons and protons give no Cherenkov photons and are thus distinguished from pions and leptons, but not from each other), but above 8 GeV/c it distinguishes kaons from all other charged particles, again by measuring the radius of the ring of detected Cherenkov photons. A complete description of the RICH detector is given in [17].

During the first part of the period of data taking concerned (1991 to 1993), the VD [18] consisted of three cylinders of silicon strip detectors, at average radii of 6.3, 9 and 11 cm. Each cylinder measured the $R\phi$ coordinates of charged particle tracks intersecting it with a precision of $\pm 8\mu$m. The association of this detector to the central tracking system of DELPHI, consisting of the TPC and the Inner and Outer Detectors, gave a precision of $\sqrt{20^2 + (65/p_T)^2}$ μm (where p_T is in GeV/c units) on the impact parameters of charged particles with respect to the primary vertex. For data registered in 1994, the inner and the outer shells of the VD were equipped with double sided detectors, provid-

ing also accurate z measurements. However, for both 1991-1993 and 1994 data, the B decay length L was estimated from $L = L_{xy}/\sin(\theta_B)$, where L_{xy} is the measured distance between the primary and the B decay vertex in the plane transverse to the beam direction and θ_B is the polar angle of the B flight direction, estimated from the B decay products.

3 The $D_s^{\pm} - \ell^{\mp}$ analysis

In this analysis, the $\overline{B}_s^0$ lifetime was measured using D_s^+ mesons correlated with a lepton of opposite charge with high transverse momentum p_t^{out} emitted in the same hemisphere:

$\overline{B}_s^0 \longrightarrow D_s^+ \ell^- \overline{\nu} X.$

3.1 D_s^+ *selection*

D_s^+ mesons were identified in three decay modes:

$D_s^+ \longrightarrow \phi\pi^+$, $\phi \longrightarrow K^+K^-$;
$D_s^+ \longrightarrow \overline{K}^{*0}K^+$, $\overline{K}^{*0} \longrightarrow K^-\pi^+$;
$D_s^+ \longrightarrow K_S^0K^+$, $K_S^0 \longrightarrow \pi^+\pi^-$.

Candidate $D_s^+ \to \phi\pi^+$ and $\overline{K}^{*0}K^+$ decays were reconstructed by making all possible combinations of three charged particles in the same event hemisphere and imposing the following kinematic cuts (some cuts were tuned differently in 91-93 and 94 data to make optimal use of the identification given by the RICH which was fully operational only in 1994):
$D_s^+ \to \phi\pi^+$:

- $p(K^{\pm}) > 1$ GeV/c and $p(\pi^+) > 1$ GeV/c ,
- $|M(\phi) - M_{PDG}(\phi)| < 9$ MeV/c^2,
- $p(\phi) > 4$ GeV/c,
- $p(D_s^+) > 6$ GeV/c.

$D_s^+ \to \overline{K}^{*0}K^+$:

- $p(K^-)$ and $p(\pi^+) > 1$ GeV/c, $p(K^+) > 2$ (1) GeV/c for 91-93 (94) data,
- $|M(\overline{K}^{*0}) - M_{PDG}(\overline{K}^{*0})| < 50$ MeV/c^2,
- $p(\overline{K}^{*0}) > 5$ (4) GeV/c for 91-93 (94) data,
- $p(D_s^+) > 7$ GeV/c.

where p is the momentum, M the reconstructed mass, and the subscript PDG indicates world average values [19]. Each track had also to be associated to at least one hit in the silicon vertex detector (VD) and the three tracks were tested for geometrical compatibility with a single vertex by imposing the very loose requirement [3] that $\chi^2(D_s^+ \text{ vertex}) < 40$. Particle identification, based on information from the Cherenkov detectors and on the energy loss measured by the TPC, was used to reduce the combinatorial background. For $D_s^+ \longrightarrow \phi\pi^+$ decays, at least one of the two kaons was selected by the "very loose" [4] identification criterion of the standard DELPHI algorithm [12, 17]. For $D_s^+ \longrightarrow \overline{K}^{*0}K^+$ decays, the bachelor kaon (K^+) was identified "very loosely" for 91-93 data and "loosely" for 94, while the other kaon was identified as at least:

- a "standard" kaon if
  40 MeV/c^2 $< |M(\overline{K}^{*0}) - M_{PDG}(\overline{K}^{*0})| < 50$ MeV/c^2,
- a "loose" kaon if
  30 MeV/c^2 $< |M(\overline{K}^{*0}) - M_{PDG}(\overline{K}^{*0})| < 40$ MeV/c^2,
- "a very loose" kaon if
  $|M(\overline{K}^{*0}) - M_{PDG}(\overline{K}^{*0})| < 30$ MeV/c^2,

and the kaon identification was used as a veto for the pion coming from $\overline{K}^{*0}$.

The background was further reduced by considering the angular distribution of the three particles involved in the decay. Since the D_s^+ is a pseudoscalar, its two body decay is isotropic, whereas the background consists of random track combinations that are more asymmetric. Hence $\cos(\eta) > -0.9$ (-0.8) was required, where η is the angle, in the D_s^+ rest frame, between the π^+ (K^+) direction and the D_s^+ line of flight in the laboratory frame. Moreover, since in the considered decay modes the pseudoscalar D_s^+ meson decays into a vector $\phi(\overline{K}^{*0})$ and a pseudoscalar meson $\pi^+(K^+)$, helicity conservation implies that the distribution of the angle ψ, in the vector meson rest frame, between the directions of its decay products and that of the pseudoscalar meson π^+ (K^+), follows a $\cos^2\psi$ dependence. Events were therefore selected by requiring $|\cos(\psi)| > 0.5$ (0.4) for 91-93 (94) data.

The $D_s^+ \to K_S^0K^+$ decay was selected by reconstructing $K_S^0 \to \pi^+\pi^-$ decays accompanied by a "very loosely" identified charged kaon in the same hemisphere. K_S^0 candidates were obtained by considering all pairs of tracks of opposite sign, and applying the "tight" selection criteria described in [12]. The K_S^0 trajectory and the K^+ track were tested for geometrical compatibility with a single vertex by requiring $\chi^2(D_s^+ \text{ vertex}) < 20$. Since the track parameters of the K_S^0 had large measurement errors, at least one VD hit associated to the charged kaon was required in order to improve the vertex resolution. To reduce the combinatorial background the following momentum cuts were also applied: $p(K^+) > 3$ GeV/c, $p(K_S^0) > 2$ GeV/c, $p(D_s^+) > 9$ GeV/c.

3.2 $D_s - \ell$ *correlation*

Using the measured position of the D_s^+ decay vertex, the measured D_s^+ momentum, and their measurement errors, a D_s^+ pseudotrack was reconstructed and used to form a common vertex (the candidate $\overline{B}_s^0$ vertex) with an identified lepton (electron or muon) of opposite charge in the same hemisphere. The lepton was required to have high momentum ($p > 3$ GeV/c) and high transverse momentum ($p_t^{out} > 1.2$ GeV/c) to suppress fake leptons and cascade decays ($b \to c \to \ell^+$) of non-strange B hadrons; the lepton track had also to be associated to at least one hit in the VD.

Further background reduction was obtained by requiring $3.0 < M(D_s^+\ell) < 5.5$ GeV/c^2, $p(D_s^+\ell) > 14$ GeV/c and $\chi^2(\overline{B}_s^0 \text{ vertex}) < 20$. In the D_s^+ mass region, a clear excess of "right-sign" combinations ($D_s^{\pm} - \ell^{\mp}$) over "wrong-sign" combinations ($D_s^{\pm} - \ell^{\pm}$) was observed in each channel

[3] There are $2N - 3$ degrees of freedom for each vertex, where N is the number of outgoing tracks, here $N = 3$

[4] "Very loose" kaon identification means simply that the track was not identified as being due to a pion

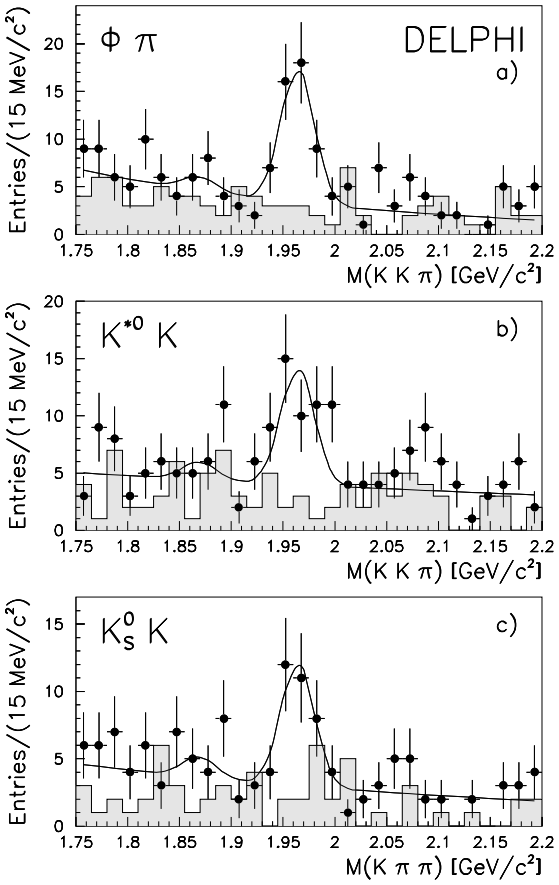

Fig. 1. $D_s\ell$ analysis: Invariant mass distributions for D_s^+ candidates, in the three analysed D_s^+ decay channels, accompanied by a lepton of opposite sign present in the same hemisphere and with p_t^{out} above 1.2 GeV/c. The "wrong-sign" combinations are given by the shaded histogram. The curves show the fit described in the text

Table 2. Numbers of D_s^+ signal events and signal to combinatorial background ratios in the three decay channels. The level of the combinatorial background was evaluated using a mass interval of $\pm 2\sigma$ centred on the measured D_s^+ mass

D_s^+ decay modes	Estimated signal	S/B ratio
$D_s^+ \longrightarrow \phi\pi^+$	37 ± 7	$\simeq 2.5$
$D_s^+ \longrightarrow \overline{K}^{*0}K^+$	27 ± 6	$\simeq 1.5$
$D_s^+ \longrightarrow K_S^0K^+$	24 ± 5	$\simeq 1.8$

(Fig. 1). For each decay channel, Table 2 gives the measured number of events in the D_s^+ signal and the ratio of the signal to the combinatorial background.

The mass distributions were fitted using two Gaussian distributions of equal widths to account for the D_s^+ and D^+ signals (the ratio between these two signals is expected to be 3 : 1) and an exponential for the combinatorial background. The D^+ mass was fixed to the nominal value of 1.869 GeV/c^2 [19]. The fit to the overall distribution, (Fig. 2), yielded a signal of 91 ± 12 D_s^+ decays in "right-sign" combinations, centred at a mass of 1.964 ± 0.003 GeV/c^2 with a width of 16 ± 2 MeV/c^2. As expected from the simulation, no signal was visible in "wrong-sign" combinations. The smaller number of "wrong-sign" than "right-sign" combinations in the background, due to local charge conservation, is also reproduced by the simulation.

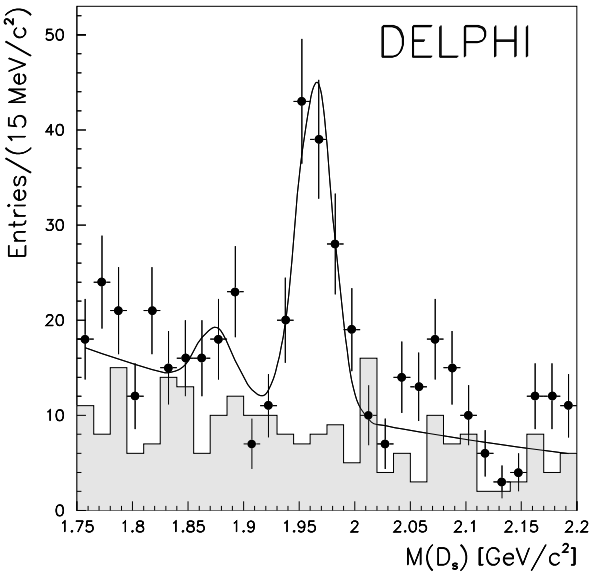

Fig. 2. $D_s\ell$ analysis: Invariant mass distribution for all D_s^+ candidates accompanied by a lepton of opposite sign present in the same hemisphere and with p_t^{out} above 1.2 GeV/c. The points with error bars correspond to "right-sign" combinations while the shaded histogram contains "wrong-sign" combinations. The curve shows the fit described in the text

3.2.1 Composition of the selected sample. The $\overline{B}_s^0$ meson lifetime was measured using the events in the "right-sign" sample lying in a mass interval of $\pm 2\sigma$ centred on the measured D_s^+ mass. The fraction of events in this sample due to the combinatorial background was evaluated from the fit to the mass distribution of "right-sign" events. It was found to be $f_{comb} = 0.356 \pm 0.071$.

There are several contributions to the D_s^+ mass peak. The signal part corresponds to D_s^+ from $\overline{B}_s^0$ semileptonic decays, for which the rate per hadronic Z decay is expected to be [5]:

$$N_{\overline{B}_s^0} = 2 \times R_{b\bar{b}} \times \mathrm{Br}(b \rightarrow \overline{B}_s^0 \rightarrow D_s^+\ell^-\overline{\nu}) \times \mathrm{Br}(D_s^+ \rightarrow \phi\pi^+)$$

which according to Table 2 is given by:

$$N_{\overline{B}_s^0} = 2 \times R_{b\bar{b}} \times \ B_1.$$

In addition to the signal part, the following background contributions were considered:

– The cascade decay $B \rightarrow \overline{D}^{(\star)}D_s^{(\star)+}X$ followed by the semileptonic decay $\overline{D}^{(\star)} \rightarrow \ell^-\overline{\nu}X$ gives "right-sign" $D_s^\pm - \ell^\mp$ pairs. This production rate can be written:

$$N_{D_s^+\overline{D}} = 2 \times R_{b\bar{b}} \times \mathrm{Br}(b \rightarrow B_{u,d} \rightarrow D_s^+X) \times Br(D_s^+ \rightarrow \phi\pi^+) \times Br(\overline{D} \rightarrow \ell X).$$

Using for $\mathrm{Br}(D \rightarrow \ell X)$ the inclusive rate of leptons from cascade decays measured at LEP (B_{bcl}) it follows that:

$$N_{D_s^+\overline{D}} = 2 \times R_{b\bar{b}} \times B_2 \times B_{bcl}.$$

About the same number of "right-sign" events is produced from this source of background as from the signal

[5] The following equations are written for the particular decay mode $D_s^+ \rightarrow \phi\pi^+$. Similar expressions hold for the other decay modes used

(Table 2). However the selection efficiency is lower for cascade decays than for direct B semileptonic decays because of the requirement of a high p_t^{out} lepton: the ratio of the two efficiencies is $R_{\mathrm{D_s^+\overline{D}}} = 0.127 \pm 0.025$.

– A $\mathrm{D_s^{\pm}}\ell^{\mp}$ pair from non-strange B meson decay, with the lepton emitted from direct B semileptonic decay, may come from the decay $\overline{\mathrm{B}} \to \mathrm{D_s}^+\mathrm{KX}\ell^-\nu$. The production of $\mathrm{D_s^+}$ in B decays not originating from $W^+ \to c\overline{s}$, has been measured by CLEO [20], but no measurement of this production in semileptonic decays exists yet. This process implies the production of a $\mathrm{D}^{\star\star}$ followed by its decay into $\mathrm{D_s K}$. This decay is suppressed by phase space (the $\mathrm{D_s}$ K system has a large mass) and by the additional $s\overline{s}$ pair required. A detailed calculation shows that the contribution of this process is [21]:

$$\frac{\mathrm{Br}(b \to \overline{\mathrm{B}} \to \mathrm{D_s^+KX}\ell^-\overline{\nu})}{\mathrm{Br(b} \to \overline{\mathrm{B}}_\mathrm{s}^0 \to \mathrm{D_s^+}\ell^-\overline{\nu})} < 10\%.$$

This contribution will be neglected in the following.

– $\mathrm{D}^+ \to \mathrm{K}^-\pi^+\pi^+$ and $\mathrm{D}^+ \to \mathrm{K_S^0}\pi^+$ decays in which a π^+ is misidentified as a K^+ are expected to give candidates in the $\mathrm{D_s^+}$ mass region. If the D^+ is accompanied by an oppositely charged lepton in the decay $\overline{\mathrm{B}}_{\mathrm{u,d}} \to \mathrm{D}^+\ell^-\overline{\nu}\mathrm{X}$, it simulates a $\overline{\mathrm{B}}_\mathrm{s}^0$ semileptonic decay. The contribution from reflections can be estimated from:

$$N_{refl} = 2 \times R_{b\overline{b}} \times \mathrm{Br}(\overline{\mathrm{B}}_{u,d} \to \mathrm{D}^+\ell^-\overline{\nu}X) \times \mathrm{Br}(\mathrm{D}^+ \to \mathrm{K}^-\pi^+\pi^+).$$

However the simulation shows that a true D^+ decaying into $\mathrm{K}\pi\pi$ would appear in the $\mathrm{KK}\pi$ hypothesis as a broad accumulation ($\simeq$ 200 MeV/c^2 wide) situated mainly above the $\mathrm{D_s^+}$ mass region. In addition the non-resonant $\mathrm{D}^+ \to \mathrm{K}^-\pi^+\pi^+$ contribution is five times larger than the resonant $\mathrm{D}^+ \to \overline{\mathrm{K}}^{\star 0}\pi^+$ one. In the simulation, after the identification cuts have been applied, the fractions of events from these kinematic reflections with respect to the $\overline{\mathrm{B}}_\mathrm{s}^0$ semileptonic decays were $R_{refl} = 0.054 \pm 0.015$ and $R_{refl} = 0.069 \pm 0.025$ in the $\overline{\mathrm{K}}^{\star 0}\mathrm{K}^+$ and the $\mathrm{K_S^0K}^+$ channels respectively.

As no excess of events was observed in the "wrong-sign" category, the possible background coming from true $\mathrm{D_s^+}$ coupled to a fake lepton was neglected.

Thus the fractions of the $\mathrm{D_s^+}$ signal due to the three main contributions are:

$$f_{\overline{\mathrm{B}}_\mathrm{s}^0} = \frac{B_1}{B_1 \times (1 + R_{refl}) + B_2 \times B_{bcl} \times R_{\mathrm{D_s^+\overline{D}}}},$$

$$f_{\mathrm{D_s^+\overline{D}}} = \frac{B_2 \times B_{bcl} \times R_{\mathrm{D_s^+\overline{D}}}}{B_1 \times (1 + R_{refl}) + B_2 \times B_{bcl} \times R_{\mathrm{D_s^+\overline{D}}}},$$

$$f_{refl} = 1 - f_{\overline{\mathrm{B}}_\mathrm{s}^0} - f_{\mathrm{D_s^+\overline{D}}}.$$

Using the values of Table 2 it follows that for the $\phi\pi$ decay mode

$$f_{\overline{\mathrm{B}}_\mathrm{s}^0} = 0.89 \pm 0.03.$$

Due to the contribution from kinematic reflection, $f_{\overline{\mathrm{B}}_\mathrm{s}^0}$ is slightly lower for the other two channels.

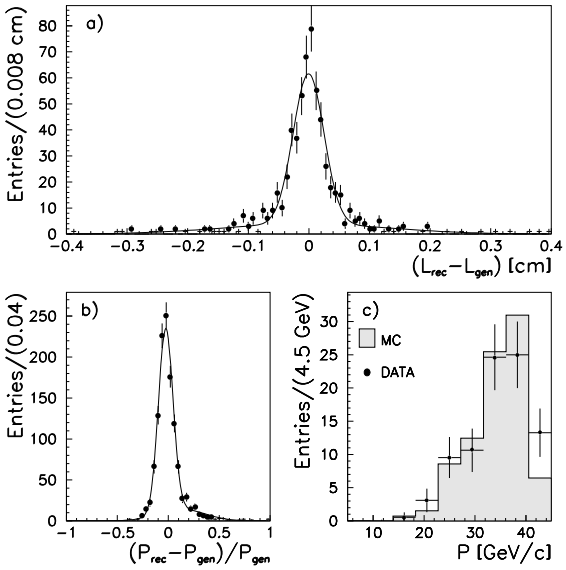

Fig. 3. $\mathrm{D_s}\ell$ analysis: $\overline{\mathrm{B}}_\mathrm{s}^0$ decay length **a)** and momentum **b)** resolution for the $\phi\pi^+$ and $\overline{\mathrm{K}}^{\star 0}\mathrm{K}^+$ decay modes of the $\mathrm{D_s^+}$. The curves show the fits described in the text. **c)** Comparison between the momentum distribution from simulated events and that estimated from real data by subtracting the momentum distribution of events in the $\mathrm{D_s^+}$ side bands from that of the events in the signal region

3.3 Lifetime measurement

3.3.1 Evaluation of the $\overline{\mathrm{B}}_\mathrm{s}^0$ decay proper time. For each event, the $\overline{\mathrm{B}}_\mathrm{s}^0$ decay proper time was obtained from the measured decay length ($L_{\overline{\mathrm{B}}_\mathrm{s}^0}$) and the estimate of the B_s momentum ($p_{\overline{\mathrm{B}}_\mathrm{s}^0}$) using the relation:

$$t = \frac{L_{\overline{\mathrm{B}}_\mathrm{s}^0} m_{\overline{\mathrm{B}}_\mathrm{s}^0}}{p_{\overline{\mathrm{B}}_\mathrm{s}^0}}.$$

The corresponding error σ_t was obtained from the errors on $L_{\overline{\mathrm{B}}_\mathrm{s}^0}$ and $p_{\overline{\mathrm{B}}_\mathrm{s}^0}$.

As indicated previously, the $\overline{\mathrm{B}}_\mathrm{s}^0$ decay length $L_{\overline{\mathrm{B}}_\mathrm{s}^0}$ was estimated from $L_{\overline{\mathrm{B}}_\mathrm{s}^0} = L_{xy}/\sin(\theta_{\overline{\mathrm{B}}_\mathrm{s}^0})$, where L_{xy} is the measured distance between the primary and the $\overline{\mathrm{B}}_\mathrm{s}^0$ decay vertex in the plane transverse to the beam direction and $\theta_{\overline{\mathrm{B}}_\mathrm{s}^0}$ is the polar angle of the $\overline{\mathrm{B}}_\mathrm{s}^0$ flight direction, as estimated from the $\mathrm{D_s^+}$–ℓ momentum vector. The distribution of the difference between the generated and reconstructed decay lengths in simulated $\phi\pi^+$ and $\overline{\mathrm{K}}^{\star 0}\mathrm{K}^+$ decays was fitted with a double Gaussian distribution, giving widths of 269 μm and 1.4 mm for 77% and 23% of the events respectively (Fig. 3a). Widths of 343 μm and 2.3 mm for 52% and 48% of the events were found in the $\mathrm{K}^0_S\mathrm{K}^+$ channel. These estimates were obtained after a tuning procedure involving additional smearing of the impact parameters and broadening of the errors in the simulation to match the data more precisely [22]. The remaining difference between real and simulated data was checked using events which, with a high probability, did not contain heavy flavour decays. The resolution

was studied using events with negative reconstructed decay lengths, for which resolution effects should dominate. After the tuning, the agreement between real and simulated data on $\sigma(L)$ was evaluated to be $\pm$10%.

The $\overline{\mathrm{B}}_{\mathrm{s}}^{0}$ momentum was estimated from:

$$p_{\overline{\mathrm{B}}_{\mathrm{s}}^{0}}{}^{2} = (E(\mathrm{D}_{\mathrm{s}}^{+}\ell) + E_{\nu})^{2} - m_{\overline{\mathrm{B}}_{\mathrm{s}}^{0}}{}^{2}.$$

The neutrino energy E_ν was evaluated from the hemisphere missing energy, defined as:

$$E_{miss} = E_{tot} - E_{vis}$$

where the visible energy (E_{vis}) is the sum of the energies of charged particles and photons in the same hemisphere as the $\mathrm{D}_{\mathrm{s}}^{+} - \ell$ candidate and E_{tot} is the total energy in that hemisphere. E_{tot} was evaluated from four momentum conservation:

$$E_{tot} = E_{beam} + \frac{M_{same}^{2} - M_{opp}^{2}}{4E_{beam}}$$

where M_{same} and M_{opp} are the hemisphere invariant masses on the same and opposite sides respectively. They were introduced to account for events in which a sizeable fraction of the centre-of-mass energy was carried away by hard gluon radiation. The neutrino energy E_ν was then calculated from E_{miss} assuming a linear dependence on the ($\mathrm{D}_{\mathrm{s}}^{+} - \ell$) energy:

$$E_{\nu} = E_{miss} + a \cdot E(\mathrm{D}_{\mathrm{s}}^{+}\ell) + b.$$

The parameters $a = 0.214 \pm 0.008$ and $b = -8.78 \pm 0.30$ GeV were estimated from the simulated events. The final $\mathrm{B_s}$ momentum resolution was $\pm$8.0% (see Fig. 3b). The relative error on the $\overline{\mathrm{B}}_{\mathrm{s}}^{0}$ momentum was parameterized as a decreasing function of the $\overline{\mathrm{B}}_{\mathrm{s}}^{0}$ momentum itself:

$$\frac{\sigma(p_{\overline{\mathrm{B}}_{\mathrm{s}}^{0}})}{p_{\overline{\mathrm{B}}_{\mathrm{s}}^{0}}} = \alpha - \beta p_{\overline{\mathrm{B}}_{\mathrm{s}}^{0}}$$

where $\alpha = 0.20 \pm 0.02$ and $\beta = 0.0030 \pm 0.0005$ (GeV/c)$^{-1}$.

To check the reliability of the $\overline{\mathrm{B}}_{\mathrm{s}}^{0}$ momentum estimate, the distribution of the estimated momentum from simulated $\overline{\mathrm{B}}_{\mathrm{s}}^{0} \to \mathrm{D}_{\mathrm{s}}^{+}\ell^{-}\overline{\nu}$ events was compared with that from real data. The latter was obtained by subtracting the estimated momentum distribution of the combinatorial background, taken in the $\mathrm{D}_{\mathrm{s}}^{+}$ side bands, from that of the events in the signal region. The comparison is shown in Fig. 3c. The difference between the mean values of the two distributions is 0.1 ± 0.7 GeV /c. The error was used to evaluate the possible systematic error coming from the difference between real and simulated data in the $\overline{\mathrm{B}}_{\mathrm{s}}^{0}$ momentum evaluation.

3.3.2 Likelihood fit. The $\overline{\mathrm{B}}_{\mathrm{s}}^{0}$ lifetime and the lifetime distribution of the combinatorial background were fitted simultaneously, using a) the "right-sign" events situated within a mass interval of $\pm 2\sigma$ centred on the measured $\mathrm{D}_{\mathrm{s}}^{+}$ mass (124 $\mathrm{D}_{\mathrm{s}}^{+} - \ell$ pairs) and at the same time b) the "right-sign" events situated in the side-bands and the "wrong-sign" events in the mass region between 1.75 and 2.2 GeV/c^2 (535 events). The likelihood function used was:

$$\mathscr{L} = \prod_{i=1}^{N_{peak}^{(right-sign)}} P_{peak}(t_i, \sigma_{t_i}) \times \prod_{j=1}^{N_{comb}^{(wrong-sign+side-bands)}} P_{comb}(t_j, \sigma_{t_j}),$$

where

$$P_{peak} = (1 - f_{comb})(f_{\overline{\mathrm{B}}_{\mathrm{s}}^{0}} P_{\overline{\mathrm{B}}_{\mathrm{s}}^{0}} + f_{\mathrm{D}_{\mathrm{s}}^{+}\overline{\mathrm{D}}} P_{\mathrm{D}_{\mathrm{s}}^{+}\overline{\mathrm{D}}} + f_{refl} P_{refl}) + f_{comb} P_{comb}$$

contains four components whose relative fractions f, described in Sect. 3.2.1, were kept fixed in the fit and correspond to:

- The $\overline{\mathrm{B}}_{\mathrm{s}}^{0}$ signal, whose probability density distribution was assumed to be the convolution of a Gaussian resolution function $G(t, \sigma_t)$ with an exponential of slope corresponding to the $\overline{\mathrm{B}}_{\mathrm{s}}^{0}$ lifetime ($\tau_{\overline{\mathrm{B}}_{\mathrm{s}}^{0}}$):

  $$P_{\overline{\mathrm{B}}_{\mathrm{s}}^{0}} = G(t, \sigma_t) \bigotimes exp(t, \tau_{\overline{\mathrm{B}}_{\mathrm{s}}^{0}})$$

  where this expression stands for $\frac{1}{\sqrt{2\pi}\sigma_t \tau} \int_0^\infty e^{\frac{-(x-t)^2}{2\sigma_t^2}} \times e^{\frac{-x}{\tau}} dx$ where x is the true lifetime, t the measured one, and σ_t is the uncertainty on the measured lifetime.
- The cascade background with a probability density distribution:

  $$P_{\mathrm{D}_{\mathrm{s}}^{+}\overline{\mathrm{D}}} = G(t, \sigma_t) \bigotimes exp(t, \tau_{\mathrm{D}_{\mathrm{s}}^{+}\overline{\mathrm{D}}})$$

  where $\tau_{\mathrm{D}_{\mathrm{s}}^{+}\overline{\mathrm{D}}}$ was estimated by fitting the proper time distribution measured in simulated $\mathrm{B} \to \mathrm{D}_{\mathrm{s}}^{+}\overline{\mathrm{D}}\mathrm{X}$ candidates: $\tau_{\mathrm{D}_{\mathrm{s}}^{+}\overline{\mathrm{D}}} = (1.92 \pm 0.20)$ ps. This effective lifetime is longer than the average b lifetime because the B momentum was underestimated for these events.
- The background coming from kinematic reflections, with a probability density distribution:

  $$P_{refl} = G(t, \sigma_t) \bigotimes exp(t, \tau_{refl})$$

  where τ_{refl} was set to the average b-hadron lifetime: $\tau_{\mathrm{B}} = (1.537 \pm 0.021)$ ps [23].
- The combinatorial background, whose probability density distribution was parameterized as:

  $$P_{comb} = \alpha G(t, \sigma_t) + \beta G(t, \sigma_t) \bigotimes exp(t, \tau^{+}) + (1 - \alpha - \beta) G(t, \sigma_t) \bigotimes exp(-t, \tau^{-})$$

  to represent a prompt (zero lifetime) and also a long-living background component; the parameters α, β, τ^+ and τ^- were left free to vary in the fit and were found to be $\alpha = 0.22 \pm 0.03$, $\beta = 0.70 \pm 0.02$, $\tau^+ = 1.54 \pm 0.10$ ps, $\tau^- = 0.99 \pm 0.18$ ps. The value of τ^+ is similar to the mean B hadron lifetime, as expected due to the enrichment of the sample in $b\bar{b}$ events. The negative exponential (third term) takes into account the possibility that negative apparent decay lengths may arise from the event topology rather than from resolution effects.

As a cross–check, the fitting function for the signal was applied to a sample of simulated $\overline{\mathrm{B}}_{\mathrm{s}}^{0}$ semileptonic decays,

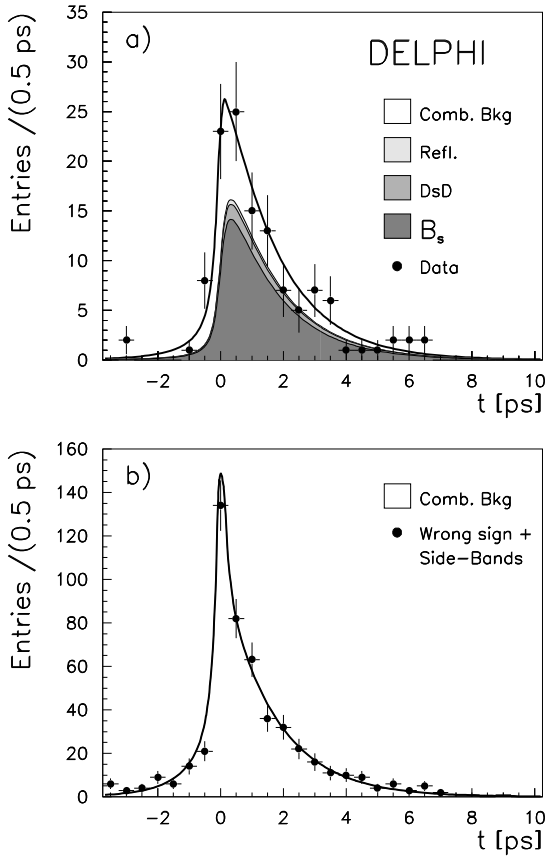

Fig. 4. $D_s\ell$ analysis: **a)** Likelihood fit for events in the signal mass region. The points show the data and the curves correspond to the different contributions to the selected events. **b)** The same as **a)** but for "wrong-sign" events and for events situated in the side band region

generated with a lifetime of 1.6 ps and passed through the same selection cuts as the real data. The lifetime obtained for this sample was 1.56 ± 0.04 ps.

Figure 4 shows the proper time distribution for real data events in the signal region and for "wrong-sign" and side-band combinations. The fitted $\overline{B}_s^0$ lifetime was found to be:

$$\tau_{\overline{B}_s^0} = \ 1.52 \ ^{+0.28}_{-0.25} \ (stat.) \text{ ps.}$$

3.3.3 Systematic errors. Systematic errors arise from uncertainties on the level and on the parameterization of the combinatorial background. This latter was evaluated by using only the wrong-sign or only the side-band events as well as different P_{comb} parameterizations. Other systematic errors come from the measured branching fractions used to calculate the fractions $f_{D_s^+\overline{D}}$ and f_{refl} in the D_s^+ signal and from the corresponding lifetimes, $\tau_{D_s^+\overline{D}}$ and τ_B. Other sets of systematic errors come from the $\overline{B}_s^0$ momentum evaluation, from the difference between real and simulated data, and from the uncertainty associated with the impact parameter rescaling. The relevant parameters were all varied by $\pm 1\sigma$, and the corresponding variations on the fitted $\overline{B}_s^0$ lifetime are reported in Table 3. Finally the lifetime was corrected by +0.04ps for the difference between the generated value

Table 3. Systematic errors on the $\overline{B}_s^0$ lifetime ($D_s\ell$ analysis)

Source of systematic error	$\tau_{\overline{B}_s^0}$ variation (ps)
f_{comb}	$^{+0.028}_{-0.024}$
P_{comb} parameterization etc.	$^{+0.036}_{-0.020}$
f_{refl}	$^{+0.006}_{-0.002}$
τ_B	± 0.002
$f_{D_s^+\overline{D}}$	$^{+0.011}_{-0.008}$
$\tau_{D_s^+\overline{D}}$	$^{+0.021}_{-0.015}$
$p_{\overline{B}_s^0}$ parameterization Data/MC	± 0.04
σ (L) rescaling Data/MC	$^{+0.005}_{-0.009}$
Possible analysis bias	± 0.04
Total	$^{+0.077}_{-0.067}$

(τ = 1.6 ps) and the value fitted in the simulated $\overline{B}_s^0$ sample (τ = 1.56$\pm$0.04 ps), since this difference was interpreted as a possible remaining bias due to limitations of the model used in the fit and the acceptance of the cuts used. The statistical error ($\pm$0.04) of this comparison was therefore included in the systematic error.

The measured $\overline{B}_s^0$ lifetime, using $D_s^\pm \ell^\mp$ candidates is thus:

$$\tau_{\overline{B}_s^0} = \ 1.56 \ ^{+0.29}_{-0.26} \ (stat.) \ ^{+0.08}_{-0.07} \ (syst.) \text{ ps.}$$

4 The $D_s^\pm - h^\mp$ analysis

This approach is similar to the $D_s^\pm - \ell^\mp$ analysis but instead of the lepton it uses a charged hadron. It provides larger statistics but suffers from an ambiguity in the choice of the hadron and from a lower $\overline{B}_s^0$ purity.

4.1 Inclusive D_s^+ *sample*

Two decay modes of the D_s^+ meson were used: $D_s^+ \to \phi\pi^+$ with $\phi \to K^+K^-$ and $D_s^+ \to \overline{K}^{*0}K^+$ with $\overline{K}^{*0} \to K^-\pi^+$. The D_s^+ candidates were reconstructed by making combinations of three charged particles in the same event hemisphere each of momentum above 1 GeV/c and associated to at least 1 VD hit. The invariant mass of the ϕ candidates had to be within ± 12 MeV/c^2 of the nominal ϕ mass and the ϕ momentum had to be larger than 5 GeV/c . Using the standard DELPHI algorithm [12, 17] for particle identification, at least one charged particle had to be at least a "loose" kaon if the K^+K^- invariant mass was within ± 4 MeV/c^2 of the nominal ϕ mass, otherwise at least one "standard" kaon was requested. The value of $|\cos(\psi)|$, defined in Sect. 3.1, had to be above 0.4. The invariant mass of the $\overline{K}^{*0}$ candidates had to be within ± 60 MeV/c^2 of the nominal $\overline{K}^{*0}$ mass value and the $\overline{K}^{*0}$ momentum had to exceed 6.5 GeV/c (4 GeV/c for 1994 data). The momentum of the bachelor kaon (K^+) had to exceed 3 GeV/c (1 GeV/c for 1994 data). To suppress the physical background from the $D^+ \to K^-\pi^+\pi^+$ reflection, the bachelor kaon (K^+) had to be identified as at least a "standard" one. For $\overline{K}^{*0} \to K^-\pi^+$ decays, the K^-

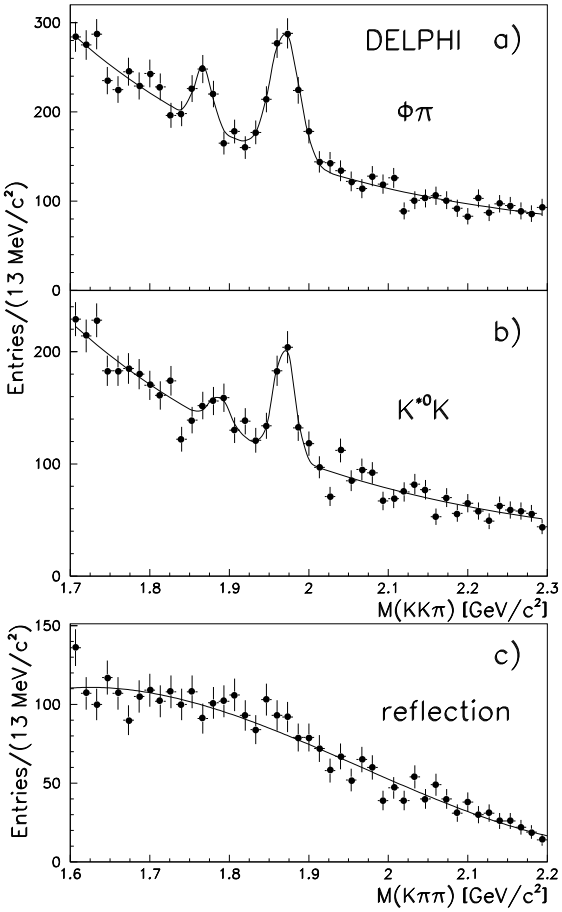

Fig. 5. $D_s h$ analysis: The invariant mass distribution for the inclusive D_s^+ samples for the **a)** $D_s^+ \to \phi\pi^+$ and **b)** $D_s^+ \to \overline{K}^{*0}K^+$ decay channels; **c)** shows the invariant mass distribution for the combinations shown in **b)** if the K^+ is assigned the π^+ mass. The curves show the fits described in the text

had to be at least "loosely" identified. The value of $|\cos(\psi)|$ had to be above 0.6 (0.8) if the mass of the $\overline{K}^{*0}$ candidate was less (more) than ± 30 MeV/c^2 from the nominal $\overline{K}^{*0}$ mass.

In both D_s^+ decay channels, the pions were chosen among the particles that were not explicitly identified as protons, kaons or leptons. The reconstructed D_s^+ decay length had to be positive and the $\chi^2(D_s^+$ vertex) had to be below 20.

Figure 5 shows the inclusive D_s^+ signals obtained in the $\phi\pi^+$ and $\overline{K}^{*0}K^+$ decay channels, and also the invariant mass distribution of the $\overline{K}^{*0}K^+$ events with the K^+ assigned the π^+ mass. The latter distribution shows that, in the selected $D_s^+ \to \overline{K}^{*0}K^+$ sample, the contribution from the $D^+ \to K^-\pi^+\pi^+$ reflection is small. The fit was performed using an exponential for the combinatorial background and two Gaussian distributions for the D_s^+ and D^+ signals: 473 ± 47 $D_s^+ \to \phi\pi^+$ events and 231 ± 32 $D_s^+ \to \overline{K}^{*0}K^+$ events were found with fitted masses of 1.970 ± 0.002 GeV/c^2 and 1.969 ± 0.002 GeV/c^2 respectively.

4.2 Selection of $D_s^\pm - h^\mp$ *events*

The procedure consisted in preselecting, using an impact parameter technique, a sample of tracks coming predominantly from B hadron decay and accompanying the D_s^+ candidate. Only tracks in the same hemisphere as the reconstructed D_s^+ were considered. This preselected sample was then used for the hadron selection, for the $\overline{B}_s^0$ enrichment and for the B momentum estimate.

4.2.1 Preselection of the tracks accompanying the D_s^+. The impact parameter δ with respect to the primary vertex is on average smaller for tracks from the primary vertex ("NB–tracks") than for tracks accompanying the D_s^+ and also arising directly or indirectly from B hadron decay ("B–tracks"). Also, the average momentum is lower for NB–tracks than for B–tracks, so the average error, $\sigma(\delta)$, is higher. Therefore the difference between NB–tracks and B–tracks can be amplified by using the combinations of the impact parameter and its error $\delta_Z/\sigma(\delta_Z)$ and $\delta_D \times \sigma(\delta_D)$, where δ_Z and δ_D are the impact parameters calculated with respect to the primary and to the D_s^+ vertex respectively. This is illustrated in Fig. 6.

The preselected sample contains the tracks satisfying the following criteria:

- at least one associated VD hit;
- $|\delta_D \times \sigma(\delta_D)| < 4.5 \times 10^{-4}$ cm^2;
- if $|\delta_D \times \sigma(\delta_D)| > 4.5 \times 10^{-4}$ cm^2 then $|\delta_Z/\sigma(\delta_Z)| > 10$ and $p_{track} > 2$ GeV/c .

In the simulation about 83% of B–tracks and 35% of NB–tracks passed these cuts.

4.2.2 Selection of the hadron candidate. The hadron was searched for amongst the preselected tracks in the event using the following criteria:

- it is not a "standard" or "tight" identified lepton with $p_t^{out} > 1$ GeV/c; if such lepton was found the whole event was rejected to reduce the correlation with the $D_s^\pm - \ell^\mp$ analysis;
- its charge is opposite to that of the D_s^+;
- it has the highest momentum among the candidates opposite in charge to the D_s^+.

In the simulation, after removing the $D_s^\pm - \ell^\mp$ candidates, the purity f_h of the selected hadron sample was found to be

$$f_h = \frac{(D_s^+ \ + \ \mathrm{B-track})}{(D_s^+ \ + \ \mathrm{B-track}) + (D_s^+ \ + \ \mathrm{NB-track})} = (83.9 \pm 3.5)\%$$

and the efficiency of the selection was about 80%.

4.2.3 Initial composition of the $D_s^\pm - h^\mp$ *sample.* The $D_s^\pm - h^\mp$ sample contains a large physics background due to D_s^+ from non-strange B hadron decays and from $c\bar{c}$ fragmentation. To estimate the relative fractions of the different D_s^+ sources, the production rate of D_s from all B species, B_L =

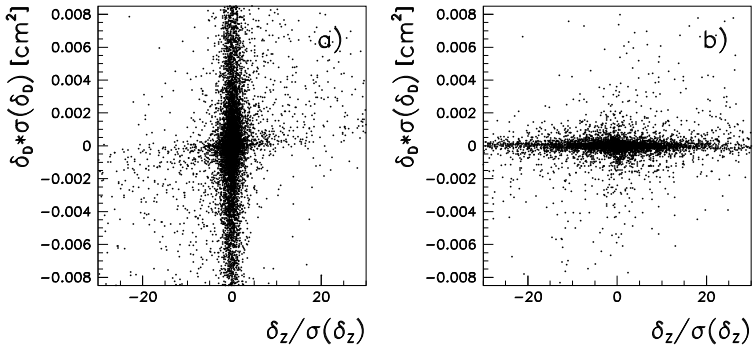

Fig. 6. $D_s h$ analysis: simulated impact parameter distributions combined with their own errors: **a)** for tracks from the primary vertex (NB–tracks) and **b)** for tracks accompanying the D_s^+ and coming directly or indirectly from the B decay (B–tracks). In both figures the impact parameter δ_Z is calculated with respect to the primary vertex while δ_D is calculated with respect to the D_s^+ vertex, $\sigma(\delta_Z)$ and $\sigma(\delta_D)$ are the corresponding errors

Br($b \to D_s^{\pm} X$) $\times$ Br($D_s^{\pm} \to \phi\pi^{\pm}$), measured by the ALEPH, DELPHI and OPAL Collaborations [4], and the equivalent quantity B_2 = Br($B_{u,d} \to D_s^{\pm} X$)$\times$Br($D_s^{\pm} \to \phi\pi^{\pm}$), measured at the $\Upsilon(4S)$ by the CLEO and ARGUS Collaborations [3], were used. Two processes contribute to the full decay rate of $\overline{B}_s^0$ into $D_s^{\pm}$. The first corresponds to $\overline{B}_s^0 \to D_s^+ X$ decays and is given by $B_L - B_2$. The second is the decay of the $\overline{B}_s^0$ into two charmed mesons, $\overline{B}_s^0 \to D_s^- DX$, and has been evaluated assuming that this mechanism has the same probability for all B hadrons. Its contribution is then given by $P_s \times B_2$. Averaging the results of the three LEP Collaborations, the production rate of $D_s^{\pm}$ from $\overline{B}_s^0$ decays was estimated to be

$$B_3 = \text{Br}(b \to \overline{B}_s^0 \to D_s^{\pm} X) \times \text{Br}(D_s^{\pm} \to \phi\pi^{\pm}) = (0.39 \pm 0.09) \times 10^{-2}.$$

The fraction of $D_s^{\pm}$ from non-strange B hadrons was found to be

$$(2 \times P_{u,d} + P_{baryon}) \times \ B_2 = (0.33 \pm 0.03) \times 10^{-2}.$$

The relative contribution from direct charm was estimated from the measurement of D_s^+ production in charm events from CLEO and ARGUS [5], taking into account the Z partial widths into b and c quarks:

$$(R_{c\bar{c}}/R_{b\bar{b}}) \times B_4 = (0.23 \pm 0.03) \times 10^{-2}.$$

The simulated event samples were weighted to agree with these measured rates.

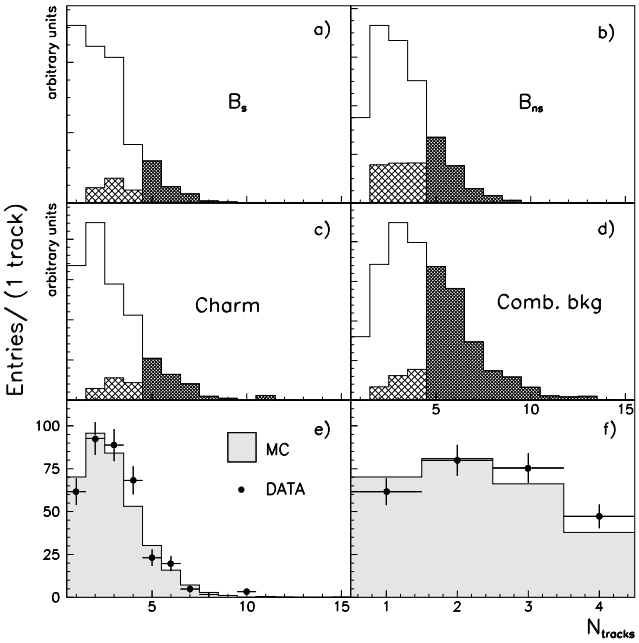

Fig. 7. $D_s h$ analysis: **a)–d)** Charged multiplicity distributions for tracks accompanying D_s^+ mesons and coming from different sources. The lightly hatched areas show the effect of removing identified "right–sign" kaons. The heavily hatched areas show the effect of the multiplicity cut. The next two figures show the charged particle multiplicity distributions after combinatorial background subtraction in the mass interval $\pm 2\sigma$ around the measured D_s^+ mass **e)** before and **f)** after applying these two cuts

4.2.4 $\overline{B}_s^0$ enrichment and final composition of the $D_s^{\pm} - h^{\mp}$ sample. To suppress the $c\bar{c}$ and light quark backgrounds, the b-tagging technique [12, 22] was applied. The probability was calculated that the tracks in the given hemisphere come from the primary vertex. Because of the long B lifetime this was much lower for events containing a B decay. In this analysis, the probability in the hemisphere opposite to the D_s^+ had to be lower than 20%. This cut kept almost 80% of the $b\bar{b}$ events and reduced the charm background by more than a factor 2.

Furthermore, simulation studies showed that the mean number of tracks accompanying a D_s^+, as defined in Sect. 4.2.1, is different for the different sources of D_s^+. Figures 7a-d show the corresponding distributions. Only decays with accompanying charged multiplicity N_{tracks} below 5 were retained, considerably suppressing the combinatorial background and also removing a larger fraction of $\overline{B}_{ns}$ (non $\overline{B}_s^0$) decays than of the $\overline{B}_s^0$ signal.

$B_{d,u} \to D_s^{(*)} D^{(*)} X$ decays are the main source of D_s^+ mesons from $\overline{B}_{ns}$ background. About 45% of the D_s^+ in these decays are accompanied by a kaon of the same charge. A "standard" or tighter identified "same–sign" kaon accompanying the D_s^+ meson was searched for and events containing such kaons were removed. This cut rejects a larger fraction of $\overline{B}_{ns}$ background than of D_s^+ from other sources (Figs. 7a-d).

The agreement between simulation and real data was verified by comparing the charged multiplicity distributions (after combinatorial background subtraction) for tracks accompanying D_s^+ mesons in the signal region, which was again taken as a mass interval of $\pm 2\sigma$ around the fitted D_s^+ mass. The shapes of these distributions (Fig. 7e,f) and the num-

Table 4. Fractions of the different components in the inclusive D_s^+ signal. The last column gives the expected composition of the selected $D_s^{\pm} - h^{\mp}$ events after applying all the cuts

D_s^+ source	Inclusive D_s^+ sample (%)	Selected $D_s^{\pm} - h^{\mp}$ sample (%)
$\overline{B}_s^0$	41.1 ± 5.9	52.7 ± 6.5
$\overline{B}_{ns}$	34.7 ± 4.1	35.5 ± 5.4
Charm	24.2 ± 3.4	11.8 ± 2.2

bers of rejected events — (26.7 ± 2.7)% in the real data and (28.8 ± 1.1)% in the $q\bar{q}$ simulation — are in agreement.

The fractions of the D_s^+ signal due to the different sources before and after applying the selection criteria[6] are given in Table 4. Uncertainties are dominated by the errors on the measured production rates (Table 2), the uncertainty coming from the simulation statistics being small. The final $\overline{B}_s^0$ purity of the sample is 0.60, whereas the fraction of charm events R_{cb}, defined as the ratio between the numbers of D_s^+ originating from charm and from beauty hadrons, is 0.13. Note that the final $\overline{B}_s^0$ purity has been noticeably improved with respect to the initial value, considering the fact that the rejection of the $D_s^{\pm} - \ell^{\mp}$ candidates, during the hadron selection, adversely affected the $\overline{B}_s^0$ purity.

Figure 8 shows the D_s^+ signals obtained after the $D_s^{\pm} - h^{\mp}$ selection. The number of D_s^+ candidates was obtained by fitting these distributions in the same way as the inclusive D_s^+ ones described in Sect. 4.1 and Fig. 5 (for the $\overline{K}^{*0}K^+$ mode only one Gaussian was used for the D_s^+ signal since in this case no clear signal of D^+ was visible). The numbers of D_s^+ events were 175 ± 25 and 86 ± 17 with fitted masses of 1.971 ± 0.002 GeV/c^2 and 1.970 ± 0.003 GeV/c^2 for the $D_s^+ \to \phi\pi^+$ and $D_s^+ \to \overline{K}^{*0}K^+$ decay modes respectively. The percentages of D_s^+ signal among the events within $\pm 2\sigma$ of the measured D_s^+ mass were (56.3 ± 8.0) % and (49.7 ± 9.8)% respectively. As was discussed in Sect. 4.1, the physical background from the $D^+ \to K^-\pi^+\pi^+$ reflection in the selected inclusive $D_s^+ \to \overline{K}^{*0}K^+$ sample is small. The reflection component in the selected $D_s^{\pm} - h^{\mp}$ sample was evaluated from simulation using the numbers quoted in Table 2 for the D^+ fraction in $c\bar{c}$ events and the probability to have a D^+ in B meson decays. Taking into account the difference in selection efficiency between the $\phi\pi^+$ and $\overline{K}^{*0}K^+$ final states, the reflection component in the selected $D_s^{\pm} - h^{\mp}$ sample was found to be (1.3 ± 0.7)%. These events come mainly from B hadron decays and their small contribution was included in the fraction of $\overline{B}_{ns}$ hadrons. The final composition of the sample of events with a D_s^+ mass situated within $\pm 2\sigma$ of the nominal mass was:

- fraction from $\overline{B}_s^0$ with correct hadron: $f_{\overline{B}_s^0}$ = (23.6 ± 4.1)%;
- fraction from $\overline{B}_{ns}$ with correct hadron: $f_{\overline{B}_{ns}}$ = (16.5 ± 3.2)%;

[6] Due to the different selection criteria for the $D_s^+ \to \phi\pi^+$ and $D_s^+ \to \overline{K}^{*0}K^+$ decay modes, the relative proportions of the D_s^+ sources are different for these two channels. The quoted $D_s^{\pm} - h^{\mp}$ sample composition was evaluated taking into account the relative numbers of events in the $D_s^+ \to \phi\pi^+$ and $D_s^+ \to \overline{K}^{*0}K^+$ channels found in the real data

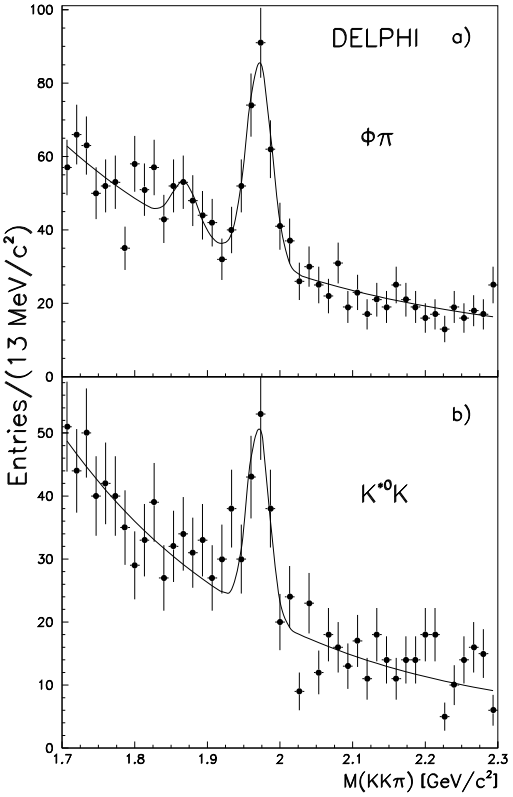

Fig. 8. $D_s h$ analysis: KKπ invariant mass distributions for the $D_s^{\pm} - h^{\mp}$ samples for **a)** $D_s^+ \to \phi\pi^+$ and **b)** $D_s^+ \to \overline{K}^{*0}K^+$. The curves show the fits described in the text

- fraction from $\overline{B}_s^0 + \overline{B}_{ns}$ with wrong hadron: $f_{\overline{B}_{\overline{h}}}$ = (7.7 ± 1.9)%;
- fraction from $c\bar{c}$ events: $f_{c\bar{c}}$ = (6.3 ± 1.4)%;
- fraction from combinatorial background: f_{comb} = (45.9 ± 6.2)%;

where "correct hadron" means a hadron coming from the B decay whereas "wrong hadron" means one from the primary vertex.

4.3 Lifetime measurement

4.3.1 Proper time measurement. The B decay vertex was reconstructed by constraining the selected hadron and the D_s^+ candidate to a common vertex. As before, the $\overline{B}_s^0$ decay length ($L_{\overline{B}_s^0}$) was estimated from $L_{\overline{B}_s^0} = L_{xy}/\sin(\theta_{\overline{B}_s^0})$, where L_{xy} is the measured distance between the primary and the $\overline{B}_s^0$ decay vertex in the plane transverse to the beam direction and $\theta_{\overline{B}_s^0}$ is the polar angle of the $\overline{B}_s^0$ flight direction, as estimated from the D_s^+–hadron momentum vector.

The ability of the simulation to reproduce the tracking resolution in the real data well was checked in the same way as in Sect. 3.3.1. The decay length resolutions obtained by fitting to a double Gaussian function were 310 μm for 64% of $\overline{B}_s^0$ and 1.7 mm for the remaining 36% (Fig. 9a), to be compared with 390 μm for 59% of $\overline{B}_{ns}$ events and 1.8 mm

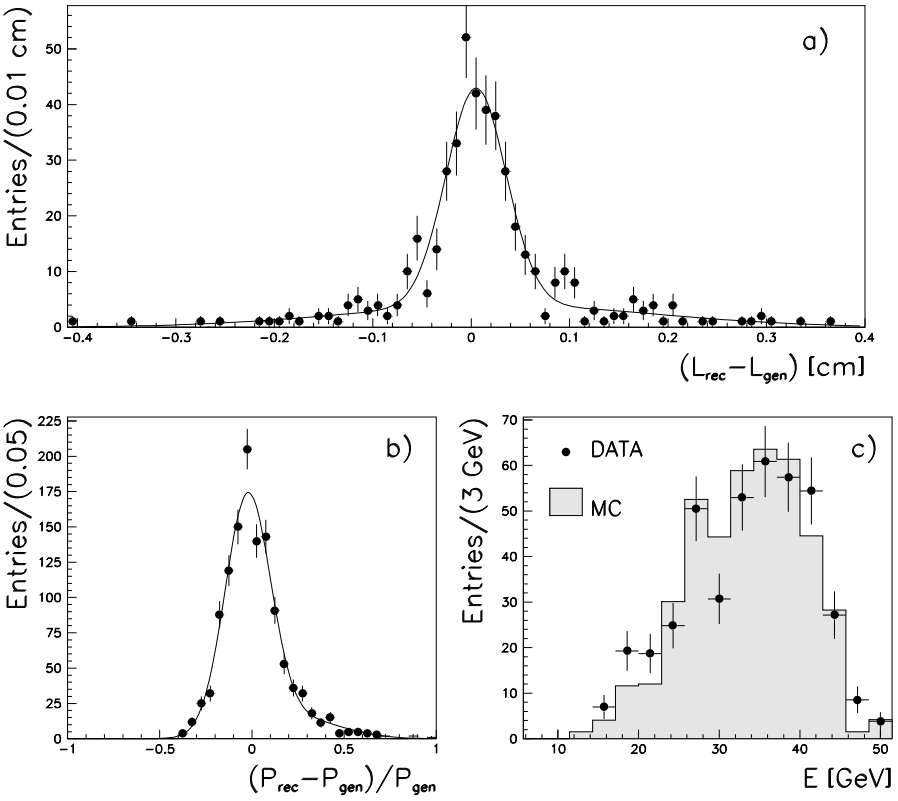

Fig. 9. $D_s h$ analysis: **a)** $\overline{B}_s^0$ decay length resolution: L_{rec} is the reconstructed decay length and L_{gen} is its generated value. **b)** The B meson momentum resolution: P_{rec} is the reconstructed momentum and P_{gen} is its generated value. Both distributions were fitted with a superimposition of two Gaussians. **c)** Comparison between the energy distribution from simulated events and that estimated from real data by subtracting the energy distribution of the events in the D_s^+ side bands from that of the events in the signal region

for the remaining 41%. Since a D_s^+ from a $\overline{B}_{ns}$ decay is emitted mainly together with another D meson, the hadron selected in these decays often did not originate directly from the B vertex, resulting in a worse resolution. In almost 50% of the $\overline{B}_{ns}$ decays, the two charmed mesons are accompanied by an extra track which can be selected in place of the D decay products. Due to the presence of $\overline{B}_s^0 \to D_s^- DX$ decays, the $\overline{B}_s^0$ sample also contains a small component in which the selected hadron comes from a second D_s decay. These different resolutions for $\overline{B}_s^0$ and for $\overline{B}_{ns}$ were taken into account in the likelihood fit.

In order to reconstruct the B hadron momentum, p_B, the momenta of the D_s^+ and of the preselected tracks, as defined in Sect. 4.2.1, were summed. A small contribution due to neutrals and tracks without VD hits, provided that their absolute value of the rapidity exceeded 1.2, was added. The rapidity was calculated as $0.5 \times \log((E + P_L)/(E - P_L))$, where E is the energy of the particle assuming the pion mass and P_L its longitudinal momentum with respect to the thrust axis of the event.

The reconstructed momentum was corrected to take into account the correlation between the resolution and the value of the momentum itself. After this correction, the overall resolution (Fig. 9b) on p_B was 13% and varied from 27% at low p_B to 6% in the high momentum region. In simulated events, the direction θ_{fl} of the reconstructed momentum was found to coincide with the true flight direction of the parent B hadron with an accuracy $\sigma_{\theta_{fl}}$ of 25 mrad. Figure 9c compares the reconstructed B energy distribution for the real events in the signal region after combinatorial background subtraction with that for the corresponding events from the $q\bar{q}$ simulation. The shapes of the distributions agree: the difference between the mean energies for the real and simulated data is 0.2 ± 0.5 GeV.

The B hadron decay proper time was estimated as in Sect. 3.3.1 and the corresponding error σ_t was obtained from the errors on the decay length and momentum.

4.3.2 Likelihood fit. The $\overline{B}_s^0$ lifetime and the time distribution of the combinatorial background were fitted simultaneously, using a) selected events in the D_s^+ peak region within $\pm 2\sigma$ of the measured D_s^+ mass (484 events) and b) combinatorial background events lying in the D_s^+ mass side–band between 2.1 and 2.3 GeV/c^2(487 events). As before, the likelihood function used was

$$\mathscr{L} = \prod_{i=1}^{N_{peak}} P_{peak}(t_i, \sigma_{t_i}) \times \prod_{j=1}^{N_{comb}} P_{comb}(t_j, \sigma_{t_j})$$

where t_i and σ_{t_i} are the measured proper time and its error for the i–th event. The probability density function for events in the peak region has the following components:

$$P_{peak} = (1 - f_{\overline{B}_{ns}} - f_{\overline{B}_{\overline{h}}} - f_{c\overline{c}} - f_{comb}) P_{\overline{B}_s^0} + f_{\overline{B}_{ns}} P_{\overline{B}_{ns}} + (f_{\overline{B}_{\overline{h}}} + f_{c\overline{c}}) P_{b,c\overline{c}} + f_{comb} P_{comb}$$

where the relative fractions f, described in Sect. 4.2.4, were kept fixed in the fit and the probability density distributions $P_{\overline{B}_s^0}$, $P_{\overline{B}_{ns}}$, $P_{b,c\overline{c}}$ and P_{comb} were as follows:

– The probability density distribution for the $\overline{B}_s^0$ signal was assumed to be an exponential of slope corresponding to

the $\overline{\mathrm{B}}_{\mathrm{s}}^{0}$ lifetime ($\tau_{\overline{\mathrm{B}}_{\mathrm{s}}^{0}}$) convoluted with a Gaussian resolution function $G(t,\sigma_t)$:

$$P_{\overline{\mathrm{B}}_{\mathrm{s}}^{0}} = G(t,\sigma_t)\bigotimes exp(t,\tau_{\overline{\mathrm{B}}_{\mathrm{s}}^{0}}).$$

– The probability density distribution for the $\overline{\mathrm{B}}_{ns}$ background was described by a similar function:

$$P_{\overline{\mathrm{B}}_{ns}} = G(t,\sigma_t)\bigotimes exp(t,\tau_{\overline{\mathrm{B}}_{ns}}).$$

The $\tau_{\overline{\mathrm{B}}_{ns}}$ fitted on the simulated data generated with a 1.6 ps lifetime was 1.578 $\pm$ 0.061 ps. Using the measured inclusive b hadron lifetime, 1.537 ± 0.021 ps, it follows that $\tau_{\overline{\mathrm{B}}_{ns}}$ = 1.516 $\pm$ 0.062 ps.

– The proper time distribution for $\mathrm{D}_{\mathrm{s}}^{+}$ from $c\bar{c}$ events was well approximated by a Gaussian centred on zero. For $\mathrm{D}_{\mathrm{s}}^{+}$ from $b\bar{b}$ events accompanied by a hadron from the interaction point, there is a small positive tail since the $\mathrm{D}_{\mathrm{s}}^{+}$ does not point back to the primary vertex but to the B hadron decay vertex. The proper time distribution for these backgrounds was taken from simulation and well described by the function

$$P_{b,c\bar{c}} = c_1 G(t,\sigma_0) + c_2 e^{-c_3 t} \quad (for\ t > 0)$$
$$c_1 G(t,\sigma_0) + c_4 e^{c_5 t} \quad (for\ t < 0).$$

All the above coefficients c_i (i = 1, 5) and σ_0 were taken from simulation and kept fixed in the fit.

– The probability density distribution for the combinatorial background was parameterized with a Gaussian plus an exponential term and with a component similar to the $\overline{\mathrm{B}}_{ns}$ probability density function for the flying (τ_{comb}) background:

$$P_{comb} = p_1 G(t,\sigma_t) + p_2 G(t,\sigma_t)\bigotimes exp(t,\tau_{comb}) + p_3 e^{-p_4 t}$$
$$(for\ t > 0)$$
$$p_1 G(t,\sigma_t) + p_5 e^{p_6 t}$$
$$(for\ t < 0).$$

where the parameters p_i (i = 1, 6) and τ_{comb} were left free to vary in the fit.

Figure 10 shows the proper time distributions for events in the signal region and for the side–band combinatorial background. The fitted $\overline{\mathrm{B}}_{\mathrm{s}}^{0}$ lifetime was found to be:

$$\tau_{\overline{\mathrm{B}}_{\mathrm{s}}^{0}} = \ 1.64\ ^{+0.34}_{-0.31}\ \mathrm{ps}.$$

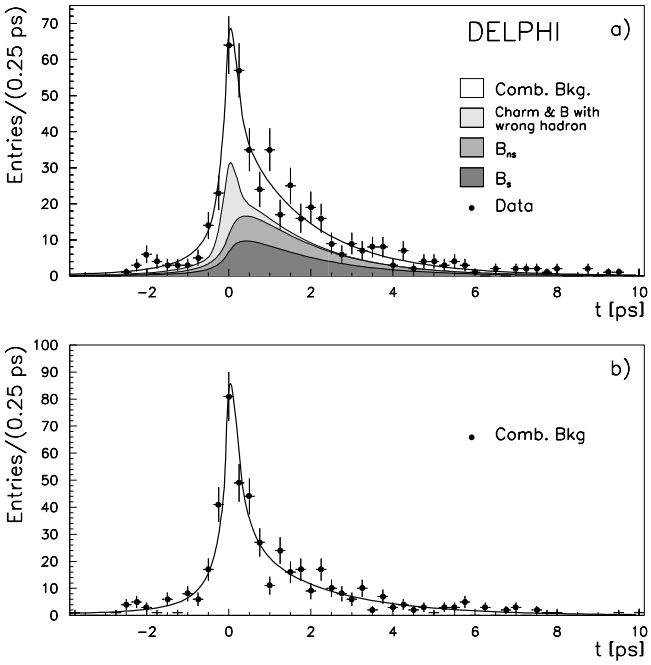

Fig. 10. $\mathrm{D_s}h$ analysis: **a)** Fitted proper time distribution for events in the signal mass region. The solid line shows the result of the maximum likelihood fit. **b)** Fitted proper time distribution for events in the side–band (2.1–2.3 GeV/c^2) mass region

Table 5. Sources of the systematic errors on the $\overline{\mathrm{B}}_{\mathrm{s}}^{0}$ lifetime ($\mathrm{D}_{\mathrm{s}}^{\pm} - h^{\mp}$ analysis)

Source of systematic error	$\tau_{\overline{\mathrm{B}}_{\mathrm{s}}^{0}}$ variation (ps)
Uncertainties in $f_{\mathrm{B}_s}, f_{\overline{\mathrm{B}}_h}, f_b, f_{c\bar{c}}$	$^{+0.059}_{-0.052}$
Uncertainty in f_{comb}	$^{+0.042}_{-0.044}$
$\overline{\mathrm{B}}_{\mathrm{s}}^{0}$ decay multiplicity	$^{+0.017}_{-0.010}$
b-tagging efficiency	$^{+0.019}_{-0.014}$
$P_{b,c\bar{c}}$ parameterization	$^{+0.014}_{-0.017}$
Momentum resolution Data/MC	$\pm$0.025
σ (L) rescaling Data/MC	$^{+0.016}_{-0.010}$
$\overline{\mathrm{B}}_{ns}$ lifetime: $\tau_{\overline{\mathrm{B}}_{ns}}$	$\pm$0.030
Analysis bias correction	$\pm$0.080
Total	$^{+0.119}_{-0.115}$

4.3.3 Systematic errors. The contributions to the systematic uncertainty on the $\overline{\mathrm{B}}_{\mathrm{s}}^{0}$ lifetime measurement are summarized in Table 5.

The systematic error due to the uncertainties in the relative fractions of the different $\mathrm{D}_{\mathrm{s}}^{+}$ sources was obtained by $\pm 1\sigma$ variation of the fractions f used in the likelihood fit, excluding f_{comb} which was studied separately. Two additional effects may have an influence on the relative fractions f. The first concerns the $\overline{\mathrm{B}}_{\mathrm{s}}^{0}$ decay multiplicity which is poorly known experimentally. It gives an uncertainty in the multiplicity distribution for the preselected tracks accompanying the $\mathrm{D}_{\mathrm{s}}^{+}$ meson. The cut imposed on N_{tracks} was varied by ± 1 for $\overline{\mathrm{B}}_{\mathrm{s}}^{0}$ events, keeping for the other $\mathrm{D}_{\mathrm{s}}^{+}$ sources the value of 5 used in the analysis. The $\overline{\mathrm{B}}_{\mathrm{s}}^{0}$ fraction varied between 21.0% and 25.2%. The second effect concerns the efficiency of the b-tagging procedure used to suppress the $c\bar{c}$ component. The $c\bar{c}$ fraction was estimated to vary between 5.4% and 7.5%.

The reflection from $\mathrm{D}^{+} \to \mathrm{K}^{-}\pi^{+}\pi^{+}$ decays was rather small and it was included in the $\overline{\mathrm{B}}_{ns}$ fraction. No significant effect on the $\overline{\mathrm{B}}_{\mathrm{s}}^{0}$ lifetime was found assuming that this reflection came totally from $c\bar{c}$ events. The procedure of removing events with the "same-sign" kaon accompanying the $\mathrm{D}_{\mathrm{s}}^{+}$ meson can bring some bias due to the possible difference in the kaon identification efficiency between real and simulated data. In the signal region after combinatorial background subtraction, the number of rejected events was found to be a factor 1.04 ± 0.03 bigger in the real data than in the

simulation. The influence of this effect on the $\overline{\mathrm{B}}_{\mathrm{s}}^{0}$ lifetime is negligible.

The coefficients $P_{b,c\bar{c}}$ taken from simulation were varied within their errors to determine the contribution to the systematic uncertainty. The systematic error coming from the possible difference between real and simulated data in the B momentum estimation was evaluated using the difference of the mean values of the two distributions discussed in Sect. 4.3.1. The lifetime of the $\overline{\mathrm{B}}_{ns}$ component fitted on the simulated data was also varied by $\pm 1\sigma$.

Finally the simulated $\overline{\mathrm{B}}_{\mathrm{s}}^{0}$ events, generated with a lifetime of 1.6 ps and passed through the same selection cuts as the real data, have a fitted lifetime of 1.59 ± 0.08 ps. The statistical error of this comparison (± 0.08) was included in the systematic error. After correcting for this possible analysis bias, the measured $\overline{\mathrm{B}}_{\mathrm{s}}^{0}$ lifetime was found to be

$$\tau_{\overline{\mathrm{B}}_{\mathrm{s}}^{0}} = 1.65\ ^{+0.34}_{-0.31}\ (stat.)\ \pm 0.12\ (syst.)\ \mathrm{ps}.$$

5 The ϕ-lepton analysis

This analysis is more inclusive and uses events where a high p_t^{out} lepton is accompanied by a ϕ meson in the same jet. The high p_t^{out} lepton enriches the sample in direct semileptonic decays and the presence of the ϕ enriches its $\overline{\mathrm{B}}_{\mathrm{s}}^{0}$ purity to around 50%.

5.1 Selection of ϕ - lepton events

The analysis was limited to 1993 and 1994 data. The ϕ meson was reconstructed through the $\phi \rightarrow \mathrm{K^+K^-}$ decay mode. The charged particles of the event were separated into two hemispheres with respect to the thrust axis. The invariant mass was calculated for all pairs of particles, assumed to be kaons, with opposite charge and situated in the same hemisphere as an identified lepton, The momenta of the kaon candidates had to exceed 1.5 GeV/c (2.0 GeV/c), that of the ϕ candidate had to exceed 3.5 GeV/c (4.0 GeV/c), and the invariant mass of the two tracks and the lepton had to exceed 1.7 $\mathrm{GeV/c^2}$ (1.9 $\mathrm{GeV/c^2}$) for data taken in 1994 (1993). These kinematic cuts were made tighter for data taken in 1993 in order to obtain a similar signal to background ratio. In addition, at least one of the kaon candidates had to be identified as such by the dE/dx measurement in the TPC or by the RICH detectors (identification of both kaon candidates was required for 1993 data) [12].

Only leptons with momentum above 2 GeV/c and transverse momentum p_t^{out} larger than 1 GeV/c were considered in the analysis. The latter cut strongly suppressed the contribution from direct charm events ($\mathrm{D_s^+} \rightarrow \phi \ell^+ \nu_\ell$) and from cascade B semileptonic decays ($b \rightarrow c \rightarrow \ell^+$).

The invariant mass distribution for kaon pairs is shown in Fig. 11. It was fitted with a Breit-Wigner to account for the signal and a polynomial expression to describe the combinatorial background. The background parameterization describes well the shape of this distribution as obtained from the simulation. A signal of 433 ± 62 events was observed at a mass of $m_\phi = 1.019 \pm 0.001$ $\mathrm{GeV/c^2}$ with $\Gamma_\phi = 11.0 \pm 1.5$ MeV in agreement with the simulation prediction.

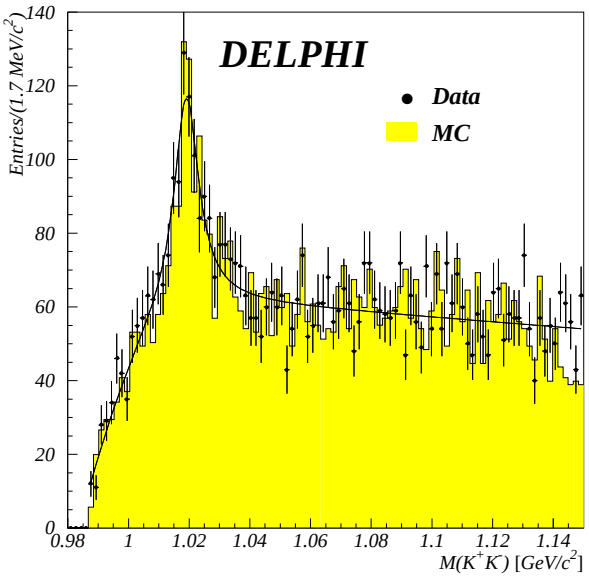

Fig. 11. $\phi\ell$ analysis: Invariant mass distribution of the kaon pair candidates. Points represent the real data, the histogram the simulated data and the full line the fitted function

5.2 Composition of the selected sample

For the measurement of the $\overline{\mathrm{B}}_{\mathrm{s}}^{0}$ lifetime, events in the ϕ meson signal region were used. The signal region corresponded to an invariant mass of the two kaon candidates between 1.008 $\mathrm{GeV/c^2}$ and 1.030 $\mathrm{GeV/c^2}$. Several mechanisms which produce a ϕ meson were studied.

Processes induced by b quarks are:

- Semileptonic decays of $\overline{\mathrm{B}}_{\mathrm{s}}^{0}$ mesons resulting in a ϕ meson in the final state through an intermediate charmed meson state. Their contribution is given by:

$$\begin{aligned} N^1_{\overline{\mathrm{B}}_{\mathrm{s}}^{0}} \ = \ & 2 \times R_{b\bar{b}} \times P_s \\ & \times (\ \mathrm{Br}(\overline{\mathrm{B}}_{\mathrm{s}}^{0} \rightarrow \mathrm{D_s^+} \ell^- \mathrm{X}) \times \mathrm{Br}(\mathrm{D_s^+} \rightarrow \phi \mathrm{X}) \\ & + \mathrm{Br}(\overline{\mathrm{B}}_{\mathrm{s}}^{0} \rightarrow \mathrm{D_{ns}} \ell^- X) \times \mathrm{Br}(\mathrm{D_{ns}} \rightarrow \phi \mathrm{X})\ ) \end{aligned}$$

  where $\mathrm{D_{ns}}$ means a non-strange D meson.
- Semileptonic decays of non-strange B mesons resulting in a ϕ meson in the final state through an intermediate charmed meson state. Their contribution is given by:

$$\begin{aligned} N^1_{\mathrm{B}} \ = \ & 2 \times R_{b\bar{b}} \times P_{u,d} \\ & \times (\ \mathrm{Br}(\mathrm{B} \rightarrow \mathrm{D}^0 \ell \mathrm{X}) \times \mathrm{Br}(\mathrm{D}^0 \rightarrow \phi \mathrm{X}) \\ & + \mathrm{Br}(\mathrm{B} \rightarrow \mathrm{D}^+ \ell \mathrm{X}) \times \mathrm{Br}(\mathrm{D}^+ \rightarrow \phi \mathrm{X})\ ). \end{aligned}$$

  Non-strange B meson semileptonic decays to a $\mathrm{D_s^+}$ are highly suppressed, as shown in Sect. 3.2.1, so they have not been included.
- Cascade decays (b→c→ ℓ^+) of strange and non-strange B mesons where the lepton and the ϕ meson are produced in semileptonic charmed meson decays. Three different processes can contribute:

1. The initial B meson is not strange and the ϕ and the ℓ are produced through decays of two different D hadrons:

$$N^2_{\rm B} = 2 \times R_{b\bar{b}} \times (P_{u,d}) \times {\rm Br(B \to D_s DX)} \times({\rm Br(D \to \ell X)} \times {\rm Br(D^+_s \to \phi X)} + {\rm Br(D_s \to \ell X)} \times {\rm Br(D \to \phi X)}\ ).$$

2. The initial B meson is a $\overline{\rm B}^0_{\rm s}$ and both the ϕ and the ℓ are produced through the decay of a $\rm D^+_s$ meson:

$$N^2_{\overline{\rm B}^0_{\rm s}} = 2 \times R_{b\bar{b}} \times P_s \times {\rm Br}(\overline{\rm B}^0_{\rm s} \to {\rm D^+_s X}) \times {\rm Br(D^+_s \to \phi \ell^+ \nu)}.$$

3. The initial B meson is not strange and both the ϕ and the ℓ are produced through the decay of a $\rm D^+_s$ meson:

$$N^3_{\rm B} = 2 \times R_{b\bar{b}} \times P_{u,d} \times {\rm Br(B \to D^+_s X)} \times {\rm Br(D^+_s \to \phi \ell^+ \nu)}.$$

The relative contributions of these processes, after imposing the cut, were determined from the simulation; when combined they yielded 0.014 ± 0.004 of the final sample.

The $\overline{\rm B}^0_{\rm s}$ purity of the sample, defined as the fraction of $\overline{\rm B}^0_{\rm s}$ decays among the selected B hadron decays, $f_{\overline{\rm B}^0_{\rm s}} = N_{\overline{\rm B}^0_{\rm s}}/(N_{\overline{\rm B}^0_{\rm s}} + N_{\rm B})$, has to be determined. To a very good approximation, it follows that $N_{\overline{\rm B}^0_{\rm s}}$ is given by the first term of $N^1_{\overline{\rm B}^0_{\rm s}}$ and that $N_{\rm B}$ is given by $N^1_{\rm B}$. These two processes are very similar from the kinematic point of view and the difference in reconstruction efficiency was found to be negligible. Thus:

$$f_{\overline{\rm B}^0_{\rm s}} = P_s \times {\rm Br}(\overline{\rm B}^0_{\rm s} \to {\rm D^+_s \ell^- X}) \times {\rm Br(D^+_s \to \phi X)} \ / \ (P_s \times {\rm Br}(\overline{\rm B}^0_{\rm s} \to {\rm D^+_s \ell^- X}) \times {\rm Br(D^+_s \to \phi X)} + P_{u,d} \times ({\rm Br(B \to D^0 \ell X)} \times {\rm Br(D^0 \to \phi X)} + {\rm Br(B \to D^+ \ell X)} \times {\rm Br(D^+ \to \phi X)})).$$

Using the values given in Table 2 and the inclusive value for the semileptonic branching fraction, which is justified because the branching ratios $\rm D^0 \to \phi X$ and $\rm D^+ \to \phi X$ are almost equal, it follows that:

$f_{B_s} = 0.50 \pm 0.07$.

The main sources of background are:

– Semileptonic decays of charmed mesons produced directly in the Z decay (only $\rm D_s$ mesons are expected to contribute to this process):

$N^f_3 = 2 \times R_{c\bar{c}} \times P_s \times Br(\rm D^+_s \to \phi \ell^+ \nu)$

where the production of strange mesons is assumed to be the same in the b and c sectors and equal to P_s. With the cuts described above the contribution of this process in the simulated sample was negligible.
– Fake leptons arising from light hadron decays and misidentification. In the simulated sample their relative contribution was $f_{fake} = 0.11 \pm 0.02$.
– Events tagged by a lepton with the ϕ meson produced as part of the original fragmentation. In the simulated sample their relative contribution was 0.030 ± 0.006.
– Combinatorial background. From the fit to this mass distribution, the fraction of such events in the signal sample was found to be $f_{comb} = 0.629 \pm 0.085$.

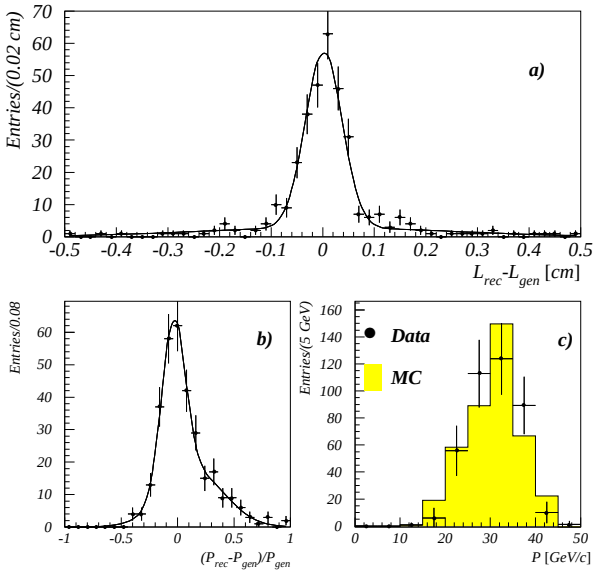

Fig. 12. $\phi\ell$ analysis: The difference between measured and generated decay distance **a)** and momentum **b)** of the $\overline{\rm B}^0_{\rm s}$ meson. **c)** Comparison of the B momentum distributions for events in the ϕ meson signal region after background subtraction: the points represent the real data and the shaded histogram the simulated sample

5.3 Lifetime measurement

5.3.1 Evaluation of the $\overline{\rm B}^0_{\rm s}$ decay proper time. A secondary $\rm K^+K^-\ell$ vertex was reconstructed and vertices with a χ^2 probability larger than 10^{-4} were retained. The decay length was determined as before. Its measurement error was inferred from simulated data to be 371 ± 28 μm (Fig. 12a). A small fraction of events ($\approx$ 6%) had a decay distance resolution of approximately 4 mm. The agreement between real and simulated data was checked as in the previous analyses. As an estimator of the $\overline{\rm B}^0_{\rm s}$ momentum, the reconstructed momentum $p(\phi\ell)$ of the $\phi - \ell$ system was used. The simulation shows that the fraction of the $\overline{\rm B}^0_{\rm s}$ momentum carried by the $\phi - \ell$ system grows linearly with the $\overline{\rm B}^0_{\rm s}$ momentum itself, according to the relation:

$$\frac{p(\phi\ell)}{p_{\overline{\rm B}^0_{\rm s}}} = a + b \times p(\phi\ell)$$

with $a = 0.203 \pm 0.065$ and $b = (1.83 \pm 0.28) \times 10^{-2}$ $(\rm GeV/c)^{-1}$. This parameterization gives the $\overline{\rm B}^0_{\rm s}$ momentum with an average error of about 16% (Fig. 12b). Figure 12c compares the momentum distribution of the reconstructed $\phi - \ell$ system obtained for simulated hadronic Z decays with the same distribution measured in real data after subtracting the combinatorial background, taken from the ϕ upper side-band. The agreement is satisfactory. The difference between the mean values of the two distributions is 0.3 ± 0.4 GeV/c. The corresponding distributions of the events in the upper side-band of the $\rm K^+K^-$ invariant mass were also compared and no significant difference was found between real and simulated data. The proper decay time and its measurement error were obtained using the same expressions as in Sect. 4.3.

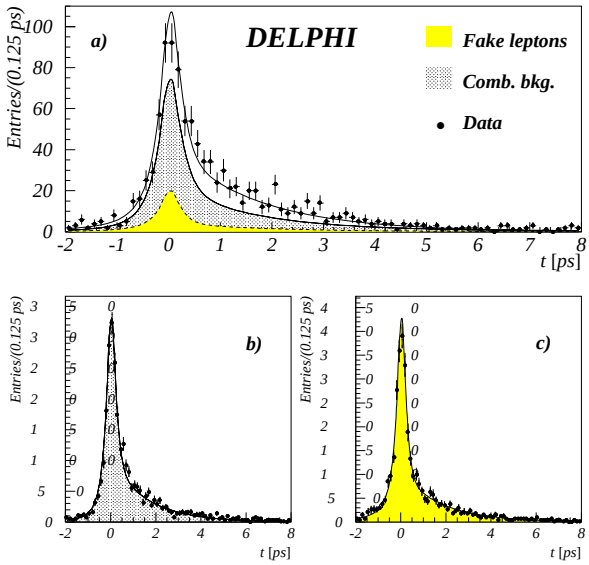

Fig. 13. $\phi\ell$ analysis: **a)** Proper decay time distribution for the events in the ϕ meson signal region: points represent the data, the line is the result of the maximum likelihood fit. The lightly shaded area shows the contribution of the combinatorial background, and the heavily shaded one the contribution from misidentified leptons or leptons from light hadron decays. **b)** Proper decay time distribution for the events in the side wing of the kaon pair invariant mass distribution. **c)** Same distribution for simulated events with either a misidentified lepton or a lepton arising from a light hadron decay

5.3.2 Likelihood fit. For events in the ϕ meson signal region, an unbinned maximum likelihood fit was performed. The following likelihood function was constructed:

$$\mathscr{L} = \prod_{i=1}^{N_{signal}} ((1-f_{comb}-f_{fake})f_{\overline{\mathrm{B}}_\mathrm{s}^0}P_{\overline{\mathrm{B}}_\mathrm{s}^0}(t_i,\sigma_{t_i},\tau_{\overline{\mathrm{B}}_\mathrm{s}^0}) + (1-f_{comb}-f_{fake})(1-f_{\overline{\mathrm{B}}_\mathrm{s}^0})P_\mathrm{B}(t_i,\sigma_{t_i},\tau_\mathrm{B}) + f_{comb}P_{comb} + f_{fake}P_{fake}).$$

– For the probability density distribution of $\overline{\mathrm{B}}_\mathrm{s}^0$ decays an exponential convoluted with a Gaussian was assumed:

$P_{\overline{\mathrm{B}}_\mathrm{s}^0}(t_i,\sigma_{t_i},\tau_{\overline{\mathrm{B}}_\mathrm{s}^0}) = G(t_i,\sigma_{t_i}) \otimes exp(t_i,\tau_{\overline{\mathrm{B}}_\mathrm{s}^0})$.

– The probability density distribution of non-strange B meson decays P_B was assumed to have the same form, but with $\tau_{\overline{\mathrm{B}}_\mathrm{s}^0}$ replaced by the average lifetime $\tau_\mathrm{B} = 1.537 \pm 0.021$ ps.

– The proper decay time distribution of the combinatorial background was parameterized as a Gaussian term for the non-flying background and the convolution of a Gaussian and an exponential for the flying background:

$$P_{comb} = f_G^{comb}G(t_i,\sigma_{t_i}) + (1-f_G^{comb})G(t_i,\sigma_{t_i}) \otimes exp(t_i,\tau_{comb}).$$

The parameters f_G^{comb} and τ_{comb} were obtained from an unbinned maximum likelihood fit to the proper decay time distribution, shown in Fig. 13b, of events in the upper side-band ($1.06\ \mathrm{GeV/c^2} \leq M_{\mathrm{K^+K^-}} \leq 1.15\ \mathrm{GeV/c^2}$) of the invariant $\mathrm{K^+K^-}$ mass distribution: $f_G^{comb} = 0.475 \pm 0.011$ and $\tau_{comb} = 1.57 \pm 0.05$ ps.

Table 6. Systematic errors on the $\overline{\mathrm{B}}_\mathrm{s}^0$ lifetime ($\phi\ell$ analysis)

Source of systematic error	$\tau_{\overline{\mathrm{B}}_\mathrm{s}^0}$ variation (ps)
Combinatorial Background (τ_{comb}, f_G^{comb})	$^{+0.12}_{-0.04}$
Fake Leptons (τ_{fake}, f_G^{fake})	$^{+0.03}_{-0.02}$
Purity (f_{B_s})	± 0.02
τ_B	± 0.01
$p_{\overline{\mathrm{B}}_\mathrm{s}^0}$ parameterization Data/MC	$^{+0.03}_{-0.03}$
Decay distance resolution Data/MC	$^{+0.03}_{-0.03}$
Possible analysis bias	± 0.08
Total	$^{+0.15}_{-0.10}$

– The contribution from events with a fake lepton was considered together with the two small contributions from events with the ϕ meson from fragmentation and events from cascade decays. The probability density distribution, P_{fake}, was constructed in the same way as P_{comb}:

$$P_{fake} = f_G^{fake}G(t_i,\sigma_{t_i}) + (1-f_G^{fake})G(t_i,\sigma_{t_i}) \otimes exp(t_i,\tau_{fake}).$$

The parameters were obtained from the fit to the corresponding proper decay time distribution obtained from simulated events (Fig. 13c): $f_G^{fake} = 0.501 \pm 0.012$, $\tau_{fake} = 1.76 \pm 0.07$ ps.

Figure 13a shows the proper decay time distribution of events in the signal region. The fitted lifetime was:

$\tau_{\overline{\mathrm{B}}_\mathrm{s}^0} = 1.74 \pm 0.20(stat.)$ ps.

As a cross–check, the fitting procedure was applied to a simulated sample containing only $\overline{\mathrm{B}}_\mathrm{s}^0$ meson decays generated with a lifetime of 1.6 ps. The fitted lifetime was 1.58 ± 0.08 ps.

5.3.3 Systematic errors. In the analysis of possible sources of systematic error, each fixed parameter of the likelihood function $\mathscr{L}$ was varied by its error. The most important were the parameters describing the combinatorial background. Other important contributions were from the difference between the real and the simulated data in the parameterization of the $\overline{\mathrm{B}}_\mathrm{s}^0$ momentum and the flight distance. As in the previous analyses, the lifetime was corrected by the difference between the generated and fitted values on the simulated data, in this case $+0.02 \pm 0.08$ ps. Including the systematic error, the $\overline{\mathrm{B}}_\mathrm{s}^0$ lifetime was found to be:

$\tau_{\overline{\mathrm{B}}_\mathrm{s}^0} = 1.76 \pm 0.20(stat.)^{+0.15}_{-0.10}(syst.)$ ps.

6 The inclusive $\mathrm{D_s^+}$ analysis

This last analysis used events containing simply a $\mathrm{D_s}^+$ meson. The $\mathrm{D_s^+} \to \phi\pi^+$ and $\mathrm{D_s^+} \to \overline{\mathrm{K}}^{*0}\mathrm{K}^+$ decay modes were used.

6.1 Selection of $\mathrm{D_s^+} \to \phi\pi^+$ *and* $\overline{\mathrm{K}}^{*0}\mathrm{K}^+$ *events*

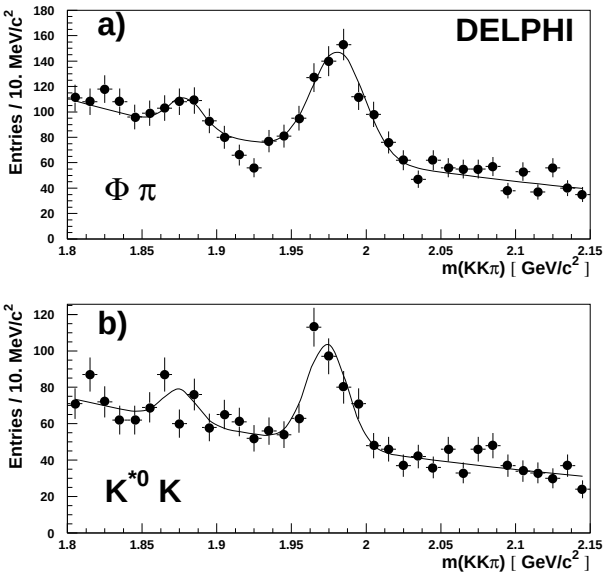

Fig. 14. Inclusive D_s analysis: $KK\pi$ mass distribution for D_s^+ candidates decaying into **a)** $\phi\pi$ and **b)** $\overline{K}^{*0}K^+$. The fit is the sum of two Gaussian distributions to describe the D_s and D peaks and an exponential to describe the background

6.1.1 $D_s^+ \to \phi\pi^+$. All charged particles forming a D_s^+ candidate had to have momentum above 1 GeV/c and at least one associated hit in the VD to give an accurate decay vertex reconstruction. The K^+K^- invariant mass had to be in the range $1.013\ \mathrm{GeV/c^2} \leq M_{K^+K^-} \leq 1.027\ \mathrm{GeV/c^2}$ and the momenta of the K^+K^- and $K^+K^-\pi^+$ systems had to be larger than 5 GeV/c and 8 GeV/c respectively. The values of $\cos(\eta)$ and $|\cos(\psi)|$ were required to be greater than -0.8 and ≥ 0.4 respectively. Fake D_s^+ were suppressed by requesting the χ^2 probability of the $K^+K^-\pi^+$ vertex to be larger than 1%. The decay length $L = L_{xy}/\sin(\theta_{D_s^+})$ had to exceed 1 mm, where L_{xy} is the measured distance between the primary and the D_s^+ decay vertex in the plane transverse to the beam direction and $\theta_{D_s^+}$ is the polar angle of the D_s^+ candidate. Both kaons were required to be loosely identified. Figure 14a shows the obtained D_s^+ signal. The number of D_s^+ candidates was measured by fitting this distribution using an exponential dependence for the combinatorial background and Gaussian distributions for the D_s^+ and D signals. The mass and width of the D_s^+ signal were left as free parameters in the fit. The total number of D_s^+ candidates was found to be 342 ± 41.

6.1.2 $D_s^+ \to \overline{K}^{*0}K^+$. As before, all charged particles forming a D_s^+ candidate had to have momentum above 1 GeV/c and at least one hit associated in the VD. The $\overline{K}^{*0}$ candidates were considered if the $K^\pm\pi^\mp$ invariant mass was in the range $0.84\,\mathrm{GeV/c^2} \leq M_{K^\pm\pi^\mp} \leq 0.94\,\mathrm{GeV/c^2}$. The momenta of the $K^\pm\pi^\mp$ and of the $K^+K^-\pi^+$ systems had to exceed 3 GeV/c and 8 GeV/c respectively. As for the $\phi\pi$ channel, the cuts on the two angular distributions were $\cos(\eta) > -0.8$ and $|\cos(\psi)| \geq 0.4$ and the χ^2 of the D_s^+ vertex had to exceed 0.01. Finally the decay length $L = L_{xy}/\sin(\theta_{D_s^+})$ had to be larger than 0.7 mm. The main contamination in the D_s^+ signal region comes from D^+ mesons decaying into $K^-\pi^+\pi^+$ with the pion mistaken as a kaon. To reduce this contamination to a negligible level, good particle identification was required by selecting only "tight" kaons; this provides a rejection factor larger than 30 against pions. The effect of this identification was verified on data and found to be in agreement with the simulation. Figure 14b shows the D_s^+ signal obtained in the $\overline{K}^{*0}K^+$ decay channel. Applying the same fitting procedure as for the $\phi\pi^+$ decay channel yielded a total of 174 ± 29 candidates.

Table 7. Numbers of $D_s^+ \to \phi\pi^+$ and $\overline{K}^{*0}K^+$ candidates measured in different decay length intervals

Distance interval (cm)	$N_{D_s^+ \to \phi\pi}$
$0.1 \leq l < 0.2$	112 ± 19
$0.2 \leq l < 0.4$	114 ± 18
$0.4 \leq l < 0.8$	103 ± 16
$0.8 \leq l < 1.0$	18 ± 7
$1.0 \leq l$	18 ± 6

Distance interval (cm)	$N_{D_s^+ \to \overline{K}^{*0}K^+}$
$0.07 \leq l < 0.2$	65 ± 15
$0.2 \leq l < 0.5$	81 ± 16
$0.5 \leq l < 1.0$	37 ± 9
$1.0 \leq l$	11 ± 4

6.2 Composition of the inclusive D_s *sample*

The composition of the inclusive D_s sample before the selection cuts was as given in the first column of Table 4. For the present analysis, the ratio of the selection efficiencies for $\overline{B}_s^0$ and non-strange B hadrons decaying into a D_s^+ was found to be $\epsilon_{\overline{B}_s^0}/\epsilon_B = 1.05 \pm 0.06$ in the simulation. The $\overline{B}_s^0$ purity of the sample was therefore

$$P_{\overline{B}_s^0} = 0.57 \pm 0.06.$$

In the same way, the fraction R_{cb} of D_s decays coming from $c\bar{c}$ relative to $b\bar{b}$ given in Table 4 was corrected by the ratio of the efficiencies, 1.11 ± 0.04 and 1.05 ± 0.08 for $\phi\pi^+$ and $\overline{K}^{*0}K^+$ respectively. It follows that:

$$R_{cb} = 0.29 \pm 0.05 \ \ (\phi\pi^+), \qquad R_{cb} = 0.30 \pm 0.06 \ \ (\overline{K}^{*0}K^+).$$

6.3 Lifetime measurement

6.3.1 Fitting procedure. The $\overline{B}_s^0$ meson lifetime was determined from the decay length distribution of the D_s^+ mesons. For each decay length interval, the number of D_s^+ candidates over the combinatorial background was measured by fitting the mass distributions in the $\phi\pi^+$ and $\overline{K}^{*0}K^+$ decay channels respectively. The decay length distributions of these fitted signals, shown in Fig. 15, were then compared to predictions from a simulation in which the B meson lifetime was varied to obtain the best fit to the data. The parameters $P_{\overline{B}_s^0}$ and R_{cb} were fixed at their central values and the corresponding uncertainties were included in the systematic errors.

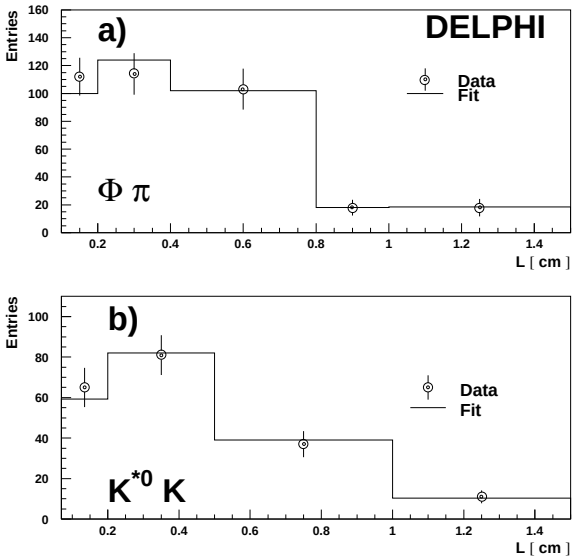

Fig. 15. Inclusive D_s analysis: Flight distance distributions for the D_s^+ signal. The points represent the data and the histogram shows the result of the fit

To measure the $\overline{B}_s^0$ lifetime, five distance intervals were defined for the $\phi\pi^+$ channel and four for the $\overline{K}^{*0}K^+$ channel. Table 7 gives the numbers of events in the D_s^+ signal, together with their associated errors, for both channels. The flight distance distributions were fitted using a simplified simulation which took into account the D_s^+ momentum distribution, the B momentum spectrum for a given D_s^+ momentum, and a Gaussian smearing of 360 $\pm$ 80 μm on the D_s^+ decay distance. The result was

$\tau(\overline{B}_s^0) = 1.58 \pm 0.26$ ps.

The method was also applied to a simulated sample of D_s^+ mesons produced in $\overline{B}_s^0$ events. The input $\overline{B}_s^0$ lifetime in this sample was 1.6 ps and the D_s^+ lifetime was 0.44 ps. The result obtained was 1.58 $\pm$ 0.08 ps. The same fit performed on D_s^+ mesons produced in non strange B ($\overline{B}_{ns}$) decays gave 1.60 $\pm$ 0.06 ps.

6.3.2 Evaluation of systematic errors. The various sources of systematic errors and their contribution to the fitted lifetime are given in Table 8. R_{cb} was varied by one standard deviation around its central value, as was the $\overline{B}_s^0$ purity of the sample. The average lifetime for the non strange B mesons was varied by the error on the value fitted in the simulated data. The uncertainty on the D_s^+ lifetime was taken from [19]. The parameters describing the momentum of the D_s^+ taken from the simulation for the $c\bar{c}$ component were varied by their statistical errors in an uncorrelated way. The error on the mean momentum fraction taken by beauty or charmed hadrons during the fragmentation of b and c quarks was taken into account by changing the ϵ_b and ϵ_c parameters in the Peterson fragmentation function by one standard deviation around their measured values. The decay length resolution was varied in the simulation by $\pm$80 μm. Finally the lifetime was corrected for the difference between the generated value (τ = 1.6 ps) and the value fitted in the simulated $\overline{B}_s^0$ sample (τ = 1.58 $\pm$ 0.08 ps) since this difference was interpreted as a possible remaining bias coming from limitations of the model fitted and the cuts used. The statistical error ($\pm$0.08 ps) of this comparison was therefore included in the systematic error. Including the systematic errors,

$\tau_{\overline{B}_s^0}$ = 1.60 $\pm$ 0.26 $(stat.)$ $^{+0.13}_{-0.15}$ $(syst.)$ ps.

Table 8. Sources of the systematic errors on the $\overline{B}_s^0$ lifetime (D_s inclusive analysis)

Source of systematic error	$\tau_{\overline{B}_s^0}$ variation (ps)
Uncertainties in $f_{\overline{B}_s^0}$	$^{+0.028}_{-0.039}$
Uncertainty in $R_{cb}(\phi\pi)$	$^{+0.055}_{-0.061}$
Uncertainty in $R_{cb}(\overline{K}^{*0}K^+)$	$^{+0.019}_{-0.022}$
τ(B) non strange	$^{+0.051}_{-0.050}$
$\tau(D_s)$	$^{+0.048}_{-0.050}$
P(D_s) parameterization for $c\bar{c}$ ($\phi\pi$)	$\pm$0.012
P(D_s) parameterization for $c\bar{c}$ ($\overline{K}^{*0}K^+$)	$\pm$0.010
Flight distance resolution Data/MC	$^{+0.041}_{-0.078}$
ϵ_b	$\pm$ 0.003
ϵ_c	$\pm$ 0.004
Analysis bias correction	$\pm$ 0.08
Total	$^{+0.13}_{-0.15}$

7 Conclusions

The $\overline{B}_s^0$ meson lifetime has been studied with four different and complementary methods. The following values were measured:

$\tau_{\overline{B}_s^0}$ = 1.56 $^{+0.29}_{-0.26}$ $(stat.)$ $^{+0.08}_{-0.07}$ $(syst.)$ ps $\quad D_s^\pm - \ell^\mp$

$\tau_{\overline{B}_s^0}$ = 1.65 $^{+0.34}_{-0.31}$ $(stat.)$ $\pm$ 0.12 $(syst.)$ ps $\quad D_s^\pm - h^\mp$

$\tau_{\overline{B}_s^0}$ = 1.76 $\pm$ 0.20 $(stat.)$ $^{+0.15}_{-0.10}$ $(syst.)$ ps $\quad \phi - \ell^\mp$

$\tau_{\overline{B}_s^0}$ = 1.60 $\pm$ 0.26 $(stat.)$ $^{+0.13}_{-0.15}$ $(syst.)$ ps $\quad inclusive\ D_s^+$

To combine these measurements, the statistical correlations were taken in account. They were estimated from the following fractions of common events:

Inclusive $D_s^+ \longleftrightarrow D_s^\pm - h^\mp$	36% of $D_s^\pm - h^\mp$ $events$
Inclusive $D_s^+ \longleftrightarrow D_s^\pm - \ell^\mp$	19% of $D_s^\pm - \ell^\mp$ $events$
Inclusive $D_s^+ \longleftrightarrow \phi - \ell^\mp$	$<$ 1% of $\phi - \ell^\mp$ $events$
$D_s^\pm - \ell^\mp \longleftrightarrow D_s^\pm - h^\mp$	6% of $D_s^\pm - \ell^\mp$ $events$
$D_s^\pm - \ell^\mp \longleftrightarrow \phi - \ell^\mp$	4% of $D_s^\pm - \ell^\mp$ $events$
$D_s^\pm - h^\mp \longleftrightarrow \phi - \ell^\mp$	$<$ 1% of $D_s^\pm - h^\mp$ $events$

where the first line means that 36 % of $D_s^\pm - h^\mp$ events were also contained in the inclusive D_s^+ sample, etc. Considering the common systematic errors (from branching ratios and lifetimes) and the above statistical correlations, the full covariance error matrix was calculated [23] and the mean $\overline{B}_s^0$ meson lifetime was found to be:

$\tau_{\overline{B}^0_s}$ = 1.67 $\pm$ 0.14 ps.

This result supersedes all previous DELPHI results for the $\overline{B}^0_s$ lifetime.

Acknowledgements. We are greatly indebted to our technical collaborators and to the funding agencies for their support in building and operating the DELPHI detector, and to the members of the CERN-SL Division for the excellent performance of the LEP collider.

References

1. P. Roudeau and A. Stocchi, "Inclusive branching fractions of D^0, D^+ and D_s into ϕ mesons", Orsay Internal Note, LAL 93-03.
2. P. Abreu et al. DELPHI Coll., Phys. Lett. **B289** (1992) 199.
   P. D. Acton et al., OPAL Coll., Phys. Lett. **B295** (1992) 357.
   D. Buskulic et al., ALEPH Coll., Phys. Lett. **B361** (1995) 221.
3. CLEO Coll., "Measurements of the B $\longrightarrow$ D_s^+ + X Decays", CLEO-CONF 94-9, contribution to the XXVIIth ICHEP, Glasgow, U.K., (July 1994).
   H. Albrecht et al., ARGUS Coll., Z. Phys. **C54** (1992) 1.
4. P. D. Acton et al., OPAL Coll., Phys. Lett. **B295** (1992) 357.
   P. Abreu et al., DELPHI Coll., Z. Phys. **C61** (1994) 407.
   D. Buskulic et al., ALEPH Coll., Z. Phys. **C69** (1996) 585.
5. W. Chen et al., CLEO Coll., Phys. Lett. **B226** (1989) 192.
   H. Albrecht et al., ARGUS Coll., Z. Phys. **C54** (1992) 1.
6. ALEPH, DELPHI, L3 and OPAL, "Combined Preliminary Data on Z Parameters from the LEP Experiments and Constraints on the Standard Model", CERN-PPE/94-187;
   ALEPH, DELPHI, L3 and OPAL, "A Combination of Preliminary LEP Electroweak Measurements and Constraints on the Standard Model", CERN-PPE/95-172.
7. M. Acciarri et al., L3 Coll., Phys. Lett. **B335** (1994) 542.
   R. Akers et al., OPAL Coll., Z. Phys. **C60** (1993) 199.
   ALEPH Coll., "Measurement of B^0_d B^0_d Oscillation Frequency", EPS0409 contribution to the ICHEP95, (Brussels, July 1995).
   DELPHI Coll., "Improved Measurements of the oscillation frequencies of the B^0 mesons", EPS0568 contribution to the ICHEP95, (Brussels, July 1995).
   R. Akers et al., OPAL Coll., Phys. Lett. **B336** (1994) 585.
   R. Akers et al., OPAL Coll., Z. Phys. **C66** (1995) 555.
   (OPAL Coll.) "An updated measurement of the B_d oscillation frequency using $D^\star$, lepton and jet charge", EPS0275 contribution to the ICHEP95, (Brussels, July 1995).
8. H. Albrecht et al., ARGUS Coll., Phys. Lett. **B207** (1988) 109.
   H. Albrecht et al., ARGUS Coll., Phys. Lett. **B269** (1991) 243.
   H. Albrecht et al., ARGUS Coll., Phys. Lett. **B274** (1992) 239.
   H. Albrecht et al., ARGUS Coll., Z. Phys. **C56** (1992) 1.
   P. Avery et al., CLEO Coll., Phys. Rev. Lett. **65** (1990) 2842.
   P. Avery et al., CLEO Coll., Phys. Rev. **D43** (1991) 3599.
9. ALEPH, DELPHI, L3 and OPAL, "Combining Heavy Flavour Electroweak Measurements at LEP", CERN-PPE/96-17.
10. P. Roudeau, "Heavy Quark Physics", Plenary talk at the XXVIIth ICHEP, Glasgow, U.K., (July 1994).
11. P. Aarnio et al. DELPHI Coll., Nucl. Instr. and Methods **A303** (1991) 233.
12. P. Abreu. et al., DELPHI Coll., "Performance of the DELPHI Detector", CERN-PPE/95-194, to be published in Nucl. Instr. and Methods.
13. T. Sjöstrand, Comp. Phys. Comm. **27** (1982) 243; ibid. **28** (1983) 229; T. Sjöstrand, M. Bengtsson, Comp. Phys. Comm. **43** (1987) 367.
14. DELPHI Coll., "Tuning and test of fragmentation based on identified particles and precision event shape data", EPS0548, contribution to the ICHEP95 (Brussels, July 1995) and paper to be submitted to Z. Phys. **C**.
15. N. Isgur, D. Scora, B. Grinstein and M. Wise, Phys. Rev. **D39** (1989) 799.
16. DELSIM Reference Manual, DELPHI internal note, DELPHI 87-97 PROG-100.
17. E.G. Anassontzis et al., Nucl. Instr. and Methods **A323** (1992) 351.
18. N. Bingefors et al., Nucl. Instr. and Methods **A328** (1993) 447.
19. L. Montanet et al., Review of Particle Properties, Phys. Rev. **D50** (1994) 1173.
20. CLEO Coll., "D_s^+-Lepton Charge Correlations in B Meson Decays: A Study of the D_s^+ Meson Production Mechanism", EPS0169 contribution to the ICHEP95, (Brussels, July 1995).
21. E. Golowich, A. Le Yaouanc, L. Oliver, O. Pène and J.C. Raynal, Z. Phys. **C48** (1990) 89;
    A. Stocchi, Ph. D. Thesis, LAL 93-10 (May 1993).
22. G.V. Borisov and C. Mariotti, 'Fine Tuning of the Impact Parameter Resolution in the DELPHI Detector', to be published in Nucl. Instr. Meth. **A**.
23. LEP B Lifetimes Working Group, "Averaging lifetimes for B hadron species at LEP", DELPHI Internal Note, DELPHI 94–164 PHYS 467 (1994).